Atmos. Chem. Phys., 15, 13195–13216, 2015
www.atmos-chem-phys.net/15/13195/2015/
doi:10.5194/acp-15-13195-2015

Atmospheric Chemistry and Physics Open Access EGU

On the ability of RegCM4 regional climate model to simulate surface solar radiation patterns over Europe: an assessment using satellite-based observations

G. Alexandri[1,2], A. K. Georgoulias[3,4,5], P. Zanis[3], E. Katragkou[3], A. Tsikerdekis[3], K. Kourtidis[2], and C. Meleti[1]

[1]Laboratory of Atmospheric Physics, Physics Department, Aristotle University of Thessaloniki, 54124 Thessaloniki, Greece
[2]Laboratory of Atmospheric Pollution and Pollution Control Engineering of Atmospheric Pollutants, School of Engineering, Democritus University of Thrace, 67100 Xanthi, Greece
[3]Department of Meteorology and Climatology, School of Geology, Aristotle University of Thessaloniki, 54124 Thessaloniki, Greece
[4]Multiphase Chemistry Department, Max Planck Institute for Chemistry, 55128 Mainz, Germany
[5]Energy, Environment and Water Research Center, The Cyprus Institute, Nicosia, Cyprus

Correspondence to: G. Alexandri (alexang@auth.gr)

Received: 18 May 2015 – Published in Atmos. Chem. Phys. Discuss.: 8 July 2015
Revised: 3 November 2015 – Accepted: 10 November 2015 – Published: 27 November 2015

Abstract. In this work, we assess the ability of RegCM4 regional climate model to simulate surface solar radiation (SSR) patterns over Europe. A decadal RegCM4 run (2000–2009) was implemented and evaluated against satellite-based observations from the Satellite Application Facility on Climate Monitoring (CM SAF), showing that the model simulates adequately the SSR patterns over the region. The SSR bias between RegCM4 and CM SAF is +1.5 % for MFG (Meteosat First Generation) and +3.3 % for MSG (Meteosat Second Generation) observations. The relative contribution of parameters that determine the transmission of solar radiation within the atmosphere to the deviation appearing between RegCM4 and CM SAF SSR is also examined. Cloud macrophysical and microphysical properties such as cloud fractional cover (CFC), cloud optical thickness (COT) and cloud effective radius (Re) from RegCM4 are evaluated against data from CM SAF. Generally, RegCM4 underestimates CFC by 24.3 % and Re for liquid/ice clouds by 36.1 %/28.3 % and overestimates COT by 4.3 %. The same procedure is repeated for aerosol optical properties such as aerosol optical depth (AOD), asymmetry factor (ASY) and single-scattering albedo (SSA), as well as other parameters, including surface broadband albedo (ALB) and water vapor amount (WV), using data from MACv1 aerosol climatology, from CERES satellite sensors and from ERA-Interim reanalysis. It is shown here that the good agreement between RegCM4 and satellite-based SSR observations can be partially attributed to counteracting effects among the above mentioned parameters. The potential contribution of each parameter to the RegCM4–CM SAF SSR deviations is estimated with the combined use of the aforementioned data and a radiative transfer model (SBDART). CFC, COT and AOD are the major determinants of these deviations on a monthly basis; however, the other parameters also play an important role for specific regions and seasons. Overall, for the European domain, CFC, COT and AOD are the most important factors, since their underestimations and overestimations by RegCM4 cause an annual RegCM4–CM SAF SSR absolute deviation of 8.4, 3.8 and 4.5 %, respectively.

1 Introduction

Modeling climate on a regional scale is essential for assessing the impact of climate change on society, the economy and natural resources. Regional climate models are limited-area models that simulate climate processes being often used to downscale dynamically global model simulations or global reanalysis data for specific regions in order to provide more detailed results (Laprise, 2008; Rummukainen, 2010). Sev-

eral studies suggest that we can benefit from the use of regional climate models, especially due to the higher resolution of stationary features like topography and coastlines and from the improved representation of small-scale processes such as convective precipitation (see Flato et al., 2013, and references therein). Usually, regional climate models are evaluated and "tuned" according to their ability to simulate temperature and precipitation (e.g., Giorgi et al., 2012; Vautard et al., 2013; Kotlarski et al., 2014). However, as discussed in Katragkou et al. (2015), the role of other climatological parameters should be included in the evaluation procedure of regional climate models (e.g., radiative fluxes, sensible and latent heat fluxes and cloud properties).

The ability of regional climate models to assess surface solar radiation (SSR) patterns has not received much attention despite the fact that SSR plays a core role in various climatic processes and parameters such as (1) evapotranspiration (e.g., Teuling et al., 2009), (2) hydrological cycle (e.g., Allen and Ingram, 2002; Ramanathan et al., 2001; Wang et al., 2010; Wild and Liepert, 2010), (3) photosynthesis (e.g., Gu et al., 2002; Mercado et al., 2009), (4) oceanic heat budget (e.g., Lewis et al., 1990; Webster et al., 1996; Bodas-Salcedo et al., 2014), and (5) global energy balance (e.g., Kim and Ramanathan, 2008; Stephens et al., 2012; Trenberth et al., 2009; Wild et al., 2013) and solar energy production (Hammer et al., 2003) and largely affects temperature and precipitation. The same holds for the parameters that drive SSR levels, such as cloud macrophysical and microphysical properties (cloud fractional cover, CFC; cloud optical thickness, COT; and cloud effective radius, Re), aerosol optical properties (aerosol optical depth, AOD; asymmetry factor, ASY; and single-scattering albedo, SSA), surface broadband albedo (ALB) and atmospheric water vapor amount (WV). However, in the last few years, there have been a few regional climate model studies focusing on the SSR levels or the net surface shortwave radiation, either to examine the dimming/brightening effect (e.g., Zubler et al., 2011; Chiacchio et al., 2015) or to evaluate the models (e.g., Jaeger et al., 2008; Markovic et al., 2008; Kothe and Ahrens, 2010; Kothe et al., 2011, 2014; Güttler et al., 2014). These studies highlight the dominating effect of cloud cover and surface albedo.

In this work, we go a step further, proceeding to a detailed evaluation of the ability of RegCM4 regional climate model to simulate SSR patterns over Europe, taking into account not only CFC and ALB but also COT, Re, AOD, ASY, SSA and WV. For the scope of this study, the same parameters are extracted from satellite-based observational data (Satellite Application Facility on Climate Monitoring (CM SAF), CERES), data from an aerosol climatology (MACv1) and data from the ERA-Interim reanalysis (see Table 1). First a decadal simulation (2000–2009) is implemented with the model and the output is evaluated against observations from the EUMETSAT geostationary satellites of CM SAF. SSR data from the Meteosat First Generation (MFG) satellites (Tessier, 1989) are available for the period 2000–2005, while data from the Meteosat Second Generation (MSG) satellites (Schmetz et al., 2002) are available for the period 2006–2009. These data are characterized by a high spatial ($\sim$ 3–5 km) and temporal resolution (15–30 min) and have been validated in the past, constituting a well-established product (e.g., Sanchez-Lorenzo et al., 2013; Posselt et al., 2014). In Sect. 2.1, the basic features of the model are described along with the simulation setup and the way various parameters are calculated by the model. In Sects. 2.2 and 2.3, a description of the satellite data from CM SAF and the other data which are used for the evaluation of RegCM4 is given, while in Sect. 2.4 we discuss the methodology followed in this paper. Section 3.1 includes the evaluation of RegCM4 SSR against data from MFG and MSG; Sects. 3.2 and 3.3 the evaluation of CFC, COT and Re against data from MSG; Sect. 3.4 the comparison of RegCM4 AOD, ASY and SSA with data from MACv1 aerosol climatology; and Sect. 3.5 the comparison of RegCM4 WV and ALB with data from ERA-Interim reanalysis and CERES satellite sensors, respectively. The CFC, COT, Re, AOD, ASY, SSA, ALB and WV data sets where chosen so as to be consistent with the CM SAF SSR data set. The potential contribution of various parameters to the RegCM4–CM SAF SSR differences is estimated with the combined use of the data mentioned above and a radiative transfer model for the MSG SSR period (2006–2009). The results are presented in Sect. 3.6, while the main findings of this paper are summarized in Sect. 4.

Table 1. List of the parameters being analyzed in this work, their sources, the original resolution at which the data were acquired and the corresponding time periods.

Parameter	Source	Resolution	Period
SSR	CM SAF MFG	$0.03° \times 0.03°$	2000–2005
SSR	CM SAF MSG	$0.05° \times 0.05°$	2006–2009
CFC	CM SAF MSG	$0.05° \times 0.05°$	2004–2009
COT	CM SAF MSG	$0.05° \times 0.05°$	2004–2009
Re	CM SAF MSG	$0.05° \times 0.05°$	2004–2009
AOD	MACv1	$1° \times 1°$	Climatology
ASY	MACv1	$1° \times 1°$	Climatology
SSA	MACv1	$1° \times 1°$	Climatology
ALB	CERES	$1° \times 1°$	Climatology
WV	ERA-Interim	$1° \times 1°$	2006–2009
All above	RegCM4	50 km $\times$ 50 km	2000–2009

2 Model description, data and methods

2.1 RegCM4 description and simulation setup

In this work, a decadal (2000–2009) simulation was implemented with RegCM4.4 (hereafter denoted RegCM4 or RegCM) for the greater European region with a horizontal resolution of 50 km. The model's domain extends from

65° W to 65° E and 15 to 75° N including the largest part of the Sahara and part of the Middle East (see Fig. S1 in the Supplement of this paper). RegCM is a hydrostatic, σ-p regional climate model with a dynamical core based on the hydrostatic version of the PSU/NCAR Mesoscale Model version 5 (MM5) (Grell et al., 1994). Specifically, RegCM4 is a substantially improved version of the model compared to its predecessor RegCM3 (Pal et al., 2007) with regard to software code and physics (e.g., radiative transfer, planetary boundary layer, convection schemes over land and ocean, land types and surface processes, ocean–air exchanges). Details on the historical evolution of RegCM from the late 1980s until today and a full description of RegCM4's basic features are given in Giorgi et al. (2012).

Data from ECMWF's ERA-Interim reanalysis were used as lateral boundary conditions. RegCM4 through a simplified aerosol scheme accounts for anthropogenic SO_2, sulfates, and organic and black carbon (Solmon et al., 2006). The emissions of these anthropogenic aerosols are based on monthly, time-dependent, historical emissions from the Coupled Model Intercomparison Project Phase 5 (CMIP5) (Lamarque et al., 2010) with a 1-year spin-up time (1999). This inventory is used by a number of climate models in support of the most recent report of the Intergovernmental Panel on Climate Change (IPCC, 2013). The model also accounts for maritime particles through a two-bin sea salt scheme (Zakey et al., 2008) and for dust through a four-bin approach (Zakey et al., 2006). For each model layer a concentration of anthropogenic SO_2, sulfates, black carbon, organic carbon, sea salt particles and dust is calculated, from which, according to a look-up table with associated optical properties, the model accounts for the aerosol extinction profiles (see Solmon et al., 2006; Zakey et al., 2006, 2008, for more details). For our simulation, the MIT–Emanuel convection scheme (Emanuel, 1991; Emanuel and Zivkovic-Rothman, 1999) was used. Convection is triggered when the buoyancy level is higher than the cloud base level. The cloud mixing is considered to be episodic and inhomogeneous, while the convective fluxes are based on a model of sub-cloud-scale updrafts and downdrafts (see Giorgi et al., 2012). Zanis et al. (2009) reported for RegCM3 that the low stratiform clouds are systematically denser and more persistent with the use of the Grell (1993) convective scheme than with the Emanuel scheme, a result with major importance for the cloud–radiation feedback. The boundary layer scheme of Holtslag et al. (1990) was utilized, while the Subgrid Explicit Moisture Scheme (SUBEX) handles large-scale cloud and precipitation computations. The ocean flux scheme was taken from Zeng et al. (1998) with the Biosphere–Atmosphere Transfer Scheme (BATS) (Dickinson et al., 1993) accounting for land surface processes.

The Community Climate Model version 3 (CCM3) (Kiehl et al., 1996) radiative package handles radiative transfer within RegCM4. The CCM3 scheme employs the δ-Eddington approximation following its predecessor (CCM2) (Briegleb, 1992). Especially for the shortwave radiation, the radiative transfer model takes into account the effect of atmospheric water vapor and greenhouse gasses, aerosol amount and optical properties per layer (e.g., aerosol optical thickness, asymmetry factor, single-scattering albedo), and cloud macrophysical (e.g., cloud fractional cover) and microphysical properties (e.g., effective droplet radius, liquid water path, cloud optical thickness) and land surface properties (surface albedo). The radiative transfer equation is solved for 18 discrete spectral intervals from 0.2 to 5 µm for the 18 RegCM vertical sigma layers from 50 hPa to the surface.

The effect of clouds on shortwave radiation is manifested by CFC, cloud droplet size and cloud water path (CWP), which is based on the prognostically calculated parameter of cloud water amount (Giorgi et al., 2012). Within the model, the effective droplet radius for liquid clouds (Rel) is considered constant (10 µm) over the ocean, while over land it is given as a function of temperature (Kiehl et al., 1998; Collins et al., 2006). On the other hand, the ice particle effective radius (Rei) is given as a function of normalized pressure, starting from 10 µm. The equations used for the calculation of Rel and Rei are given below.

$$\mathrm{Rel} = \begin{cases} 5\,\mu\mathrm{m} & T > -10\,^{\circ}\mathrm{C} \\ 5 - 5\left(\frac{T+10}{20}\right)\,\mu\mathrm{m} & -30\,^{\circ}\mathrm{C} \le T \le -10\,^{\circ}\mathrm{C} \\ \mathrm{Rei} & T < -30\,^{\circ}\mathrm{C}, \end{cases} \quad (1)$$

$$\mathrm{Rei} = \begin{cases} \mathrm{Rei}_{\min} & \\ \quad p/p_{\mathrm{s}} > p_I^{\mathrm{high}} & \\ \mathrm{Rei}_{\min} - (\mathrm{Rei}_{\max} - \mathrm{Rei}_{\min})\left[\frac{(p/p_{\mathrm{s}}) - p_I^{\mathrm{high}}}{p_I^{\mathrm{high}} - p_I^{\mathrm{low}}}\right]\,\mu\mathrm{m} & \\ \quad p/p_{\mathrm{s}} \le p_I^{\mathrm{high}}, & \end{cases} \quad (2)$$

where T is the atmospheric temperature, p is the atmospheric pressure, p_{s} is the surface pressure, $\mathrm{Rei}_{\max} = 30\,\mu\mathrm{m}$, $\mathrm{Rei}_{\min} = 10\,\mu\mathrm{m}$, $p_I^{\mathrm{high}} = 0.4$ and $p_I^{\mathrm{low}} = 0.0$. The fraction (f_{ice}) of cloud water that consists of ice particles is given as a function of T, the fraction (f_{liq}) of the liquid water droplets being calculated as $f_{\mathrm{liq}} = 1 - f_{\mathrm{ice}}$.

$$f_{\mathrm{ice}} = \begin{cases} 0 & T > -10\,^{\circ}\mathrm{C} \\ -0.05\,(T+10) & -30\,^{\circ}\mathrm{C} \le T \le -10\,^{\circ}\mathrm{C} \\ 1 & T < -30\,^{\circ}\mathrm{C} \end{cases} \quad (3)$$

Then, the radiative properties of liquid and ice clouds in the shortwave spectral region are given by the following parameterizations, originally found in Slingo (1989) and revisited

by Briegleb (1992).

$$\mathrm{COT}_{\mathrm{ph}}^{\lambda} = \mathrm{CWP}\left[a_{\mathrm{ph}}^{\lambda} + \frac{b_{\mathrm{ph}}^{\lambda}}{\mathrm{Re}_{\mathrm{ph}}}\right] f_{\mathrm{ph}}, \quad (4)$$

$$\mathrm{SSA}_{\mathrm{ph}}^{\lambda} = 1 - c_{\mathrm{ph}}^{\lambda} - d_{\mathrm{ph}}^{\lambda}\mathrm{Re}_{\mathrm{ph}}, \quad (5)$$

$$\mathrm{ASY}_{\mathrm{ph}}^{\lambda} = e_{\mathrm{ph}}^{\lambda} + f_{\mathrm{ph}}^{\lambda}\mathrm{Re}_{\mathrm{ph}}, \quad (6)$$

$$\phi_{\mathrm{ph}}^{\lambda} = \left(\mathrm{ASY}_{\mathrm{ph}}^{\lambda}\right)^2, \quad (7)$$

where superscript λ denotes the spectral interval and subscript ph denotes the phase (liquid/ice), while ϕ is the phase function of clouds. It needs to be mentioned here that all the equations presented above are given in Kiehl et al. (1998) and Collins et al. (2004) with slightly different annotation. The coefficients a–f for liquid clouds are given in Slingo (1989), while those for ice clouds are given in Ebert and Curry (1992) for the four pseudo-spectral intervals (0.25–0.69, 0.69–1.19, 1.19–2.38 and 2.38–4.00 µm) employed in the radiative scheme of RegCM. Especially for COT, in this paper we calculated this parameter for the spectral interval 0.25–0.69 µm for both liquid and ice clouds so that it is comparable to the CM SAF satellite-retrieved COT at 0.6 µm (see Sect. 2.2). Following the approach of Cess (1985), to derive the bulk COT for the whole atmospheric column, the COTs calculated for each layer are simply added. The total COT for each layer is calculated by merging the COT values for liquid and ice clouds.

Within RegCM, CFC at each layer is calculated from relative humidity and cloud droplet radius. The surface radiation flux in RegCM4 is calculated separately for the clear and cloud-covered part of the sky. The total CFC for each model grid cell is an intermediate value between the one calculated using the random overlap approach, which leads to a maximum cloud cover, and the one found by assuming a full overlap of the clouds appearing in different layers, which minimizes cloud cover. As discussed in Giorgi et al. (2012), this approach allows for a more realistic representation of surface radiative fluxes.

2.2 CM SAF satellite data

To evaluate the RegCM4 SSR simulations described previously, we use high-resolution satellite data from the SIS (surface incoming shortwave radiation) product of CM SAF. The data sets were obtained from EUMETSAT's MFG (doi:10.5676/EUM_SAF_CM/RAD_MVIRI/V001) and MSG (doi:10.5676/EUM_SAF_CM/CLAAS/V001) geostationary satellites. SSR data are available from 1983 to 2005 from six MFG satellites (Meteosat 2–7) and from 2005 onwards from MSG satellites (Meteosat 8–10). These satellites fly at an altitude of $\sim 36\,000$ km, being located at longitudes around 0° above the Equator and covering an area extending from 80° W to 80° E and from 80° S to 80° N. In the case of MFG satellites, the SSR data are retrieved from measurements with the Meteosat Visible and Infrared Instrument (MVIRI) sensor. MVIRI is a radiometer that takes measurements at three spectral bands (visible, water vapor, infrared) every 30 min. SSR is retrieved using MVIRI's broadband visible channel (0.45–1 µm) only, at a spatial resolution of ~ 2.5 km (at the sub-satellite point). The data are afterwards re-gridded on a $0.03° \times 0.03°$ regular grid.

The MagicSol–Heliosat algorithm, used for the derivation of the SSR data analyzed in this work, has been extensively described in several papers (see Posselt et al., 2011a, b, 2012, 2014; Mueller et al., 2011; Sanchez-Lorenzo et al., 2013). The algorithm includes a modified version of the original Heliosat method (Beyer et al., 1996; Cano et al., 1986). Heliosat utilizes the digital counts obtained from the visible channel to calculate the so-called effective cloud albedo. The modified version incorporates the determination of the monthly maximum normalized digital count (for each MVIRI sensor) that serves as a self-calibration parameter. To derive the clear-sky background reflection, a 7-day running average of the minimum normalized digital counts is used instead of fixed monthly mean values. This method minimizes changes appearing in the radiance data recorded by different MVIRI sensors due to the transition from one Meteosat satellite to another, ensuring a data set that is as homogeneous as possible. Then, the clear-sky irradiances are derived using the look-up-table-based clear-sky model MAGIC (Mueller et al., 2009) and finally SSR is retrieved by combining them with the effective cloud albedo.

On the other hand, MSG satellites carry the Spinning Enhanced Visible and Infrared Imager (SEVIRI), a radiometer taking measurements at 12 spectral bands (from visible to infrared) every 15 min with a spatial resolution of ~ 3 km (at the sub-satellite point). The data used here are available in a $0.05° \times 0.05°$ regular grid. The SEVIRI broadband high-resolution visible channel (HRV), which is very close to MVIRI's broadband visible channel, cannot be used for the continuation of the SSR data set, since, unlike MVIRI, it does not cover the full Earth disk. Furthermore, the use of one of SEVIRI's narrow-band visible channels directly in the same algorithm as MVIRI (MagicSol) is not feasible – firstly because of the spectral differences with MVIRI's broadband visible channel, and secondly because of the sensitivity of cloud albedo to spectral differences of the land surfaces below the clouds (especially for vegetated areas) (see Posselt et al., 2011a, 2014). In this case, an artificial SEVIRI broadband visible channel that corresponds to MVIRI's broadband visible channel is simulated following the approach of Cros et al. (2006). SEVIRI's two narrow-band visible channels (0.6 and 0.8 µm) and MVIRI's broadband channel spectral characteristics are used to establish a simple linear model. This model is afterwards applied to SEVIRI's 0.6 and 0.8 µm radiance measurements to calculate the broadband visible channel radiance (see Posselt et al., 2014, for more details).

The CM SAF SSR satellite-based product is characterized by a threshold accuracy of $15\,W\,m^{-2}$ for monthly mean data and $25\,W\,m^{-2}$ for daily data (Mueller et al., 2011; Posselt et al., 2012, 2014; Sanchez-Lorenzo et al., 2013). Posselt et al. (2012) evaluated CM SAF SSR data on a daily and monthly basis against ground-based observations from 12 BSRN (Baseline Surface Radiation Network) stations around the world, showing that both daily and monthly CM SAF data are below the target accuracy for $\sim 90\,\%$ of the stations. Specifically for Europe, Sanchez-Lorenzo et al. (2013), using monthly SSR data from 47 GEBA (Global Energy Balance Archive) ground stations, proceeded to a detailed validation of the CM SAF SSR data set for the period 1983–2005. They found that CM SAF slightly overestimates SSR by $5.2\,W\,m^{-2}$ (4.4 % in relative values). Also, the mean absolute bias was found to be $8.2\,W\,m^{-2}$, which is below the accuracy threshold of $15\,W\,m^{-2}$ ($10\,W\,m^{-2}$ for the CM SAF retrieval accuracy and $5\,W\,m^{-2}$ for the surface measurements uncertainties). Applying the standard normal homogeneity test (SNHT), Sanchez-Lorenzo et al. (2013) revealed that the MFG SSR data over Europe can be considered homogeneous for the period 1994–2005. Recently, Posselt et al. (2014) verified the results of the previous two studies by using a combined MFG-MSG SSR data set spanning from 1983 to 2010. They found that the monthly mean data set exhibits a mean bias of $+3.16\,W\,m^{-2}$ and a mean absolute bias of $8.15\,W\,m^{-2}$ compared to BSRN, which is again below the accuracy threshold of CM SAF. Also, the data set was found to be homogeneous for the period 1994–2010 in most of the investigated regions except for Africa.

To investigate the differences appearing between the RegCM4 and CM SAF SSR fields we also use CFC, COT and Re CM SAF observations from MSG satellites for the period 2004–2009. A description of this cloud optical properties product, also known as CLAAS (CLoud property dAtAset using SEVIRI), can be found in Stengel et al. (2014). The MSG NWC software package v2010 is used for the detection of cloudy pixels, the determination of their type (liquid/ice) and their vertical placement (Derrien and Le Gléau, 2005; NWCSAF, 2010). The detection of cloudy pixels is based on a multispectral threshold method incorporating parameters such us illumination (e.g., daytime, twilight, nighttime, sunglint) and type of surface. According to Kniffka et al. (2014), the CM SAF cloud mask accuracy is $\sim 90\,\%$ (successful detection of cloudy pixels for $\sim$ 90 % of the cases) when evaluated against satellite data from CALIOP/CALIPSO and CPR/CloudSat. The bias of the CFC product was found to be $+2$ and $+3\,\%$ for SEVIRI's disk when compared to ground-based data from SYNOP (lidar-radar measurements) and satellite-based data from MODIS, respectively (Stengel et al., 2014). The cloud physical properties (CPP) algorithm (Roebeling et al., 2006; Meirink et al., 2013) is used to retrieve COT at 0.6 µm, Re and CWP. The algorithm is based on the use of SEVIRI's spectral measurements at the visible (0.64 µm) and near infrared (1.63 µm) (Nakajima and King, 1990). First, COT and Re are retrieved for the cloudy pixels and then CWP is given by the following equation:

$$\mathrm{CWP_{ph}} = 2/3\rho_{\mathrm{ph}}\mathrm{Re_{ph}}\mathrm{COT_{ph}}, \quad (8)$$

where ph stands for the clouds' phase (liquid/ice) and ρ is the density of water. According to Stengel et al. (2014), the CM SAF COT bias was estimated at $-9.9\,\%$ compared to MODIS observations. The corresponding bias for CWP is $-0.3\,\%$ for liquid-phase clouds and $-6.2\,\%$ for ice-phase clouds. COT and CWP data are available from CM SAF at a spatial resolution of $0.05^\circ \times 0.05^\circ$ on a daily basis. In this work, Re values were calculated from the COT and CWP CM SAF available data using Eq. (8).

2.3 Other data

In addition to the CM SAF SSR and cloud optical properties data used for the evaluation of RegCM4, we also use ancillary data from other sources, namely AOD, ASY and SSA at 550 nm monthly climatological values from the MACv1 climatology (Kinne et al., 2013); monthly climatological broadband surface shortwave fluxes retrieved from CERES sensors aboard EOS TERRA and AQUA satellites for a 14-year period starting from March 2000 (Kato et al., 2013); and finally monthly mean total column WV data from ECMWF's ERA-Interim reanalysis (Dee et al., 2011) for the period 2006–2009. All the data were obtained at a spatial resolution of $1^\circ \times 1^\circ$. It should be mentioned that these data are similar to the ones used as input within the MAGIC clear-sky radiative transfer code (Mueller et al., 2009), which is used for the calculation of CM SAF SSR. Therefore, they can be used in order to examine the reasons for possible deviations appearing between RegCM4 and CM SAF SSR (see Sect. 2.4). To our knowledge, the uncertainty in the MACv1 aerosol parameters used here has not been reported anywhere in detail. The CERES broadband surface albedo over land exhibits a relative bias of $-2.4\,\%$ compared to MODIS. Specifically, over deserts, the relative bias drops to $-2.1\,\%$ (Rutan et al., 2009). A detailed evaluation of the ERA-Interim WV total column product does not exist. Only recently, the upper troposphere–lower stratosphere WV data were evaluated against airborne campaign measurements, showing good agreement (30 % of the observations were almost perfectly represented by the model) (Kunz et al., 2014).

2.4 Methodology

In this study, first of all, the RegCM4 SSR fields are evaluated against SSR fields from CM SAF (MFG for 2000–2005 and MSG for 2006–2009) for the European region (box region in Fig. S1). Prior to the evaluation, the model and satellite data are averaged on a monthly basis and brought to a common $0.5^\circ \times 0.5^\circ$ spatial resolution. It should be mentioned that the same temporal and spatial resolution was used for all the data

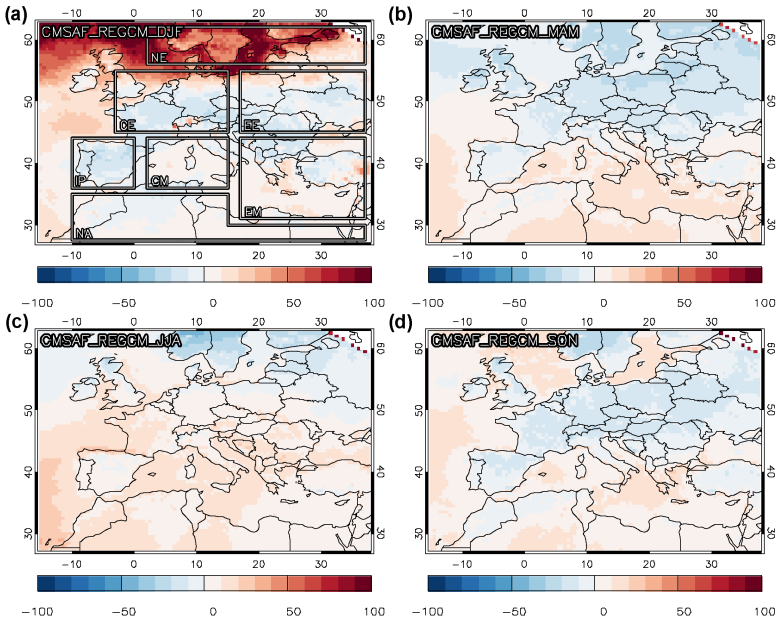

Figure 1. Seasonal NMB patterns of RegCM4–CM SAF SSR over Europe for **(a)** winter (DJF), **(b)** spring (MAM), **(c)** summer (JJA) and **(d)** autumn (SON) from MSG SEVIRI observations. The seven sub-regions used for the generalization of the results are marked in **(a)**: northern Europe (NE), central Europe (CE), eastern Europe (EE), Iberian Peninsula (IP), central Mediterranean (CM), eastern Mediterranean (EM) and northern Africa (NA).

utilized in this study. Maps with the normalized mean bias (NMB) (hereafter denoted as bias) are produced on an annual and seasonal basis. NMB is given by the following equation:

$$\mathrm{NMB} = \frac{\sum_{i=1}^{N}(\mathrm{RegCM}_i - \mathrm{CMSAF}_i)}{\sum_{i=1}^{N}\mathrm{CMSAF}_i}100\,\% = \left(\frac{\overline{\mathrm{RegCM}}}{\overline{\mathrm{CMSAF}}} - 1\right)100\,\%, \quad (9)$$

where RegCM_i and CMSAF_i represent the RegCM4 and CM SAF mean values for each month i, N is the number of months, and $\overline{\mathrm{RegCM}}$ and $\overline{\mathrm{CMSAF}}$ are the RegCM4 and CM SAF mean values. The statistical significance of the results at the 95 % confidence level is checked by means of a two-independent-sample t test:

$$t = (\overline{\mathrm{RegCM}} - \overline{\mathrm{CMSAF}})/\sqrt{\left(\sigma^2_{\mathrm{RegCM}} + \sigma^2_{\mathrm{CMSAF}}\right)/N}, \quad (10)$$

where $\sigma\mathrm{RegCM}$ and $\sigma\mathrm{CMSAF}$ are the standard deviations of RegCM4 and CM SAF total means. When $|t|$ is greater than a critical value that depends on the degrees of freedom (here $2n-1$), the bias is considered statistically significant. In addition to the whole European region (EU) and the land-covered (LA) and ocean-covered (OC) part of Europe, seven other sub-regions are defined for the generalization of our results: northern Europe (NE), central Europe (CE), eastern Europe (EE), Iberian Peninsula (IP), central Mediterranean (CM), eastern Mediterranean (EM) and northern Africa (NA) (see Figs. 1a and S1). The bias on an annual and seasonal basis is calculated per region. Apart from bias, other statistical metrics (correlation coefficient, R; normalized standard deviation, NSD; modified normalized mean bias, MNMB; root mean square error, RMSE) are also defined, calculated and presented in the Supplement of this paper. Specifically for the SSR results presented in the paper the normalized mean error (NME) is calculated along with the bias in order to get an insight into the absolute bias between the model simulations and the satellite observations.

$$\mathrm{NME} = \frac{\sum_{i=1}^{N}\left|\mathrm{RegCM}_i - \mathrm{CMSAF}_i\right|}{\sum_{i=1}^{N}\mathrm{CMSAF}_i}100\,\% \quad (11)$$

The latitudinal variability in model and satellite-based SSR and their difference is examined by means of seasonal plots. Finally, the seasonal variability in SSR from RegCM4 and CM SAF and their differences is investigated for each of the 10 regions mentioned above. While NMB is primarily used in this work for the investigation of the spatiotemporal variability in RegCM4–CM SAF deviations, the real difference is given in the plots with the latitudinal and seasonal variability for each region in order to get an insight into the performance of the model, regardless of the SSR levels. The same procedure is done separately for MFG data (2000–2005) and MSG data (2006–2009) to see whether the two data sets lead to similar results. Our results are mostly focused on MSG satellite-based observations, since CFC and cloud optical properties data are only available from MSG SEVIRI.

In order to interpret the observed differences between RegCM4 and CM SAF SSR, the same detailed procedure is repeated for CFC and COT for the period 2004–2009. CFC and COT are the two major determinants of the transmission of shortwave radiation through clouds (Gupta et al., 1993) and along with AOD constitute the major controllers of SSR (Kawamoto and Hayasaka, 2008). Therefore, we also proceed to a detailed comparison of RegCM4 AOD at 550 nm (AOD_{550}) against MACv1 climatological data. However, other cloud- (Re) and aerosol- (ASY, SSA) related parameters also play a significant role. Here, RegCM4 Re is evaluated against observational data from CM SAF, while RegCM4 ASY and SSA are compared against climatological data from MACv1 (see Supplement). Specifically, the comparison of RegCM4 data with MACv1 does not constitute an evaluation of the RegCM4 aerosol-related parameters, like in the case of the cloud-related parameters above, since MACv1 data (Kinne et al., 2013) are climatological (based on a combination of models and observations) and not pure observational data. However, a similar climatology (Kinne et al., 2006) is used for the production of CM SAF SSR (Trentmann et al., 2013). In addition, Mueller et al. (2014) showed that the use of MACv1 aerosol climatology instead of the Kinne et al. (2006) climatology does not significantly affect the CM SAF SSR product. Hence, this comparison allows us to reach useful conclusions about the effect of aerosol representation within RegCM4 on the simulated SSR fields by the model. The same holds for the comparison of RegCM4 ALB data with climatological data from CERES satellite sensors and RegCM4 WV data with WV data from ERA-Interim reanalysis (see Supplement). The CERES ALB 14-year climatology is temporally constant, similar to the CERES climatology used for the production of CM SAF SSR (Trentmann et al., 2013). Finally, the ERA-Interim WV data used here are the same as the WV data incorporated by the radiative scheme of CM SAF. Unlike the RegCM4 evaluation results, the comparison results discussed in this paragraph are presented in the Supplement.

Apart from a qualitative approach, we also proceed to a quantitative study of the reasons that could potentially lead to deviations between the RegCM4 and CM SAF SSR. Using data from RegCM4 and CM SAF and the Santa Barbara DISORT Atmospheric Radiative Transfer (SBDART) model (Ricchiazzi et al., 1998), we estimate the potential relative contribution of the parameters CFC, COT, Re, AOD, ASY, SSA, ALB and WV to the percent RegCM4–CM SAF SSR difference (ΔSSR) over the seven sub-regions mentioned above. ΔSSR is given by Eq. (12), expressing the percentage of SSR deviation caused by the observed difference between RegCM4 and CM SAF for each parameter (p). First, a SBDART simulation is implemented with a 3 h time step for the 15th day of each month (Ming et al., 2005) using monthly mean RegCM4 data as input (control run) for each region. The average of all the time steps per month expresses the monthly SSR flux ($SSR_{control}$). The SSR fields simulated with SBDART are almost identical to the RegCM4 SSR fields. This indicates that SBDART indeed can be used to study the sensitivity of RegCM4's radiative scheme to various parameters. Then, several SBDART simulations are implemented in the same way, replacing each time only one of the aforementioned input parameters with corresponding values from CM SAF, MACv1 or ERA-Interim ($SSR(p)$). $SSR_{control}$ and $SSR(p)$ are then used in Eq. (12) to calculate ΔSSR for each month (i) and parameter (p).

$$\Delta SSR^i(p) = 100\left(SSR^i_{control} - SSR^i(p)\right)/SSR^i_{control} \quad (12)$$

The results of this analysis are presented by means of bar plots for each sub-region. The procedure described above was repeated assuming the simulated SSR fields with all the CM SAF, MACv1 and ERA-Interim input data as the control run and replacing each time the corresponding parameter with data from RegCM4. This was done in order to make sure that the interdependence (the effect of changing a parameter is different under different conditions) of the examined parameters does not impact the validity of our results. In addition, a method like the one introduced by Kawamoto and Hayasaka (2008, 2010, 2011), which is based on the calculation of the sensitivities of SSR on CFC, COT, AOD and WV, was also implemented with similar results (not shown here).

3 Results and discussion

3.1 Surface solar radiation

As discussed above, we first examine the CM SAF and RegCM4 bias patterns for the MFG (2000–2005) and MSG (2006–2009) periods separately. This work focuses on the MSG data set, since cloud property data, which are used in order to investigate the reasons for the observed bias between CM SAF and RegCM4 at a later stage, are only available from MSG. However, we investigate both periods to examine whether the observed biases are valid for the whole simulation period and ensure that there are no differences when using one or the other data set. As shown in Fig. S2a and b, the annual bias patterns are similar for both MFG-RegCM4 and MSG-RegCM4. The main feature is a low negative bias over land and a low positive bias over ocean. Overall, the RegCM4 simulations slightly overestimate SSR compared to CM SAF over Europe with a bias of +1.5 % in the case of MFG and +3.3 % in the case of MSG, while SSR from RegCM4 is much closer to SSR from CM SAF over land (bias of −1.6 % for MFG and +0.7 % for MSG) than over ocean (bias of +7.2 % for MFG and +8.1 % for MSG). These values can be found in Table 2 for the RegCM4-MSG period along with the corresponding values for the seven sub-regions of interest appearing in Fig. 1a, while the same values for the RegCM4-MFG period can be found in Table S1 of the Supplement. It should be mentioned that, hereafter, only results for the MSG

Table 2. Average RegCM4 SSR and CM SAF SSR (MSG SEVIRI) with their standard deviations ($\pm 1\sigma$) and the corresponding normalized mean bias (NMB) and normalized mean error (NME) per season and region. When the difference between RegCM4 and CM SAF SSR is statistically significant at the 95 % confidence level due to a two-independent-sample t test, the NMB values are marked with bold letters, while in the opposite case they are marked with an asterisk. Positive NMBs are italic, while negative NMBs are underlined. ANN denotes annual results and DJF, MAM, JJA and SON the winter, spring, summer and autumn results, respectively.

	ANN			DJF			MAM		
	MOD	SAT	bias (NME)	MOD	SAT	bias (NME)	MOD	SAT	bias (NME)
EU	175.0 ± 106.5	169.3 ± 96.7	***3.3*** (11.7)	77.1 ± 57.1	74.2 ± 57.2	***3.9*** (13.3)	206.8 ± 83.0	206.7 ± 67.0	*0.0** (12.2)
LA	173.1 ± 106.9	171.9 ± 97.2	***0.7*** (11.7)	78.1 ± 61.0	78.0 ± 60.8	*0.1** (12.7)	202.7 ± 85.7	208.7 ± 68.6	**–2.9** (13.0)
OC	178.2 ± 105.6	164.9 ± 95.7	***8.1*** (11.8)	75.3 ± 49.7	67.7 ± 49.8	***11.3*** (14.5)	213.8 ± 77.8	203.2 ± 64.2	***5.2*** (10.9)
NE	104.0 ± 81.2	113.7 ± 93.4	**–8.5** (17.4)	19.3 ± 12.0	12.7 ± 16.8	***52.4*** (71.0)	137.6 ± 53.4	160.4 ± 60.8	**–14.2** (17.0)
CE	134.5 ± 89.2	136.1 ± 83.1	**–1.2** (14.3)	42.3 ± 20.8	42.8 ± 24.4	−1.1* (22.9)	158.1 ± 55.6	174.0 ± 51.3	**–9.1** (15.6)
EE	132.3 ± 92.0	139.5 ± 89.8	**–5.2** (12.9)	37.5 ± 17.5	38.8 ± 22.1	**–3.4** (20.1)	155.2 ± 61.2	179.4 ± 57.7	**–13.5** (16.4)
IP	197.9 ± 95.1	194.7 ± 84.4	***1.7*** (9.7)	91.7 ± 26.9	98.6 ± 27.5	**–7.0** (12.6)	224.8 ± 56.5	224.0 ± 46.3	*0.4** (9.6)
CM	209.8 ± 98.6	195.1 ± 85.1	***7.5*** (10.6)	97.3 ± 29.1	96.7 ± 27.1	*0.6** (9.1)	243.7 ± 59.2	225.9 ± 46.2	***7.9*** (11.1)
EM	219.3 ± 101.6	205.6 ± 90.3	***6.7*** (9.9)	105.1 ± 36.8	101.8 ± 33.7	***3.3*** (11.4)	251.4 ± 68.8	235.6 ± 54.4	***6.7*** (10.7)
NA	261.8 ± 82.3	243.8 ± 69.5	***7.4*** (8.9)	164.7 ± 35.2	161.8 ± 31.9	***1.8*** (6.3)	303.8 ± 41.3	280.2 ± 33.7	***8.4*** (9.3)

	JJA			SON		
	MOD	SAT	bias (NME)	MOD	SAT	bias (NME)
EU	281.6 ± 70.6	265.2 ± 55.2	***6.2*** (11.1)	126.3 ± 77.4	123.3 ± 71.3	***2.4*** (11.3)
LA	278.6 ± 71.7	267.0 ± 55.0	***4.4*** (10.7)	124.9 ± 79.0	126.1 ± 72.8	**–0.9** (11.0)
OC	286.7 ± 68.2	262.1 ± 55.3	***9.4*** (11.9)	128.7 ± 74.5	118.6 ± 68.4	***8.4*** (11.8)
NE	198.7 ± 45.5	219.4 ± 43.3	**–9.4** (13.8)	52.9 ± 38.2	53.4 ± 44.3	−1.0* (22.1)
CE	245.6 ± 47.9	228.9 ± 38.2	***7.3*** (12.0)	84.4 ± 46.8	90.9 ± 48.2	**–7.2** (13.9)
EE	248.4 ± 44.9	242.8 ± 36.5	***2.3*** (9.0)	80.1 ± 46.0	88.8 ± 48.8	**–9.8** (13.6)
IP	317.5 ± 29.1	296.3 ± 32.3	***7.2*** (8.9)	148.6 ± 53.9	151.8 ± 50.4	**–2.1** (9.6)
CM	331.3 ± 27.3	299.9 ± 25.1	***10.4*** (10.8)	157.7 ± 53.5	149.8 ± 45.4	***5.3*** (10.4)
EM	339.3 ± 29.1	312.8 ± 28.1	***8.5*** (8.9)	171.8 ± 63.0	163.7 ± 55.9	***5.0*** (9.5)
NA	353.5 ± 20.5	320.5 ± 21.7	***10.3*** (10.3)	217.2 ± 49.5	205.8 ± 39.7	***5.5*** (8.1)

CM SAF SSR data set are presented within this paper, while the results for the MFG data set are included in the Supplement (Figs. S3 to S5).

As presented in Fig. 1, some differences appear in the seasonal bias patterns. A strong positive bias is observed during winter over northern Europe. For the rest of the regions the winter patterns are very close to the spring and the annual patterns. In contrast to the annual patterns, in summer, the positive bias extends over Europe until the latitudinal zone of 50° N, while in autumn the bias patterns are quite similar to the annual ones. In winter, the RegCM4 simulations overestimate SSR compared to CM SAF for the whole European domain, the bias being +3.9 %. Over land the bias is nearly zero (+0.1 %), while over ocean there is a significant bias of +11.3 %. As shown in Fig. 1a, NE is the sub-region with by far the strongest bias (+52.4 %). Also, NME is 13.3 % for the whole European domain (12.7 % over land and 14.5 % over ocean), NE and NA being the regions with the highest (71.0 %) and lowest (6.3 %) value, respectively (Table 2). The seasonal and annual model- and satellite-derived values with the corresponding biases and NMEs and their statistical significance at the 95 % confidence level according to a two-independent-sample t test appear in Table 2. The latitudinal variability in RegCM4 SSR, CM SAF SSR and their difference is presented in Fig. 2a. As mentioned in Sect. 2.4, the differences given in the figures with the latitudinal and the seasonal variability are not normalized by the average SSR levels of each region and hence should not be confused with the bias values appearing in the text. For example, while the RegCM4–CM SAF difference is $\sim 7\,\mathrm{W\,m^{-2}}$ over NE in winter (comparable to other regions), a strong bias of ~ 52 % characterizes this region due to the low insolation levels at these latitudes. Overall, RegCM4 slightly overestimates SSR at latitudes lower than $\sim 40°$ N; a negligible difference between RegCM4 and CM SAF is observed until the latitudinal zone of $\sim 52°$ N, while a significant difference is observed for higher latitudes. In spring, a zero bias is observed between the model and CM SAF for Europe. When discriminating between land- and ocean-covered regions, a negative bias is observed over land (−2.9 %) and a positive over ocean (+5.2 %). The regions with the highest negative bias are NE (−14.2 %), EE (−13.5 %) and CE (−9.1 %), while the regions with the highest positive bias are NA (+8.4 %), CM (+7.9 %) and EM (+6.7 %) (see Table 1). This is also reflected in Fig. 2b, where RegCM4 clearly overestimates SSR for latitudes less than $\sim 44°$ N, and significantly underestimating SSR thereafter. NME is 12.2 % for the whole European domain, with 13.0 % over land and 10.9 % over ocean. NME ranges from 9.3 % (NA) to 17.0 % (NE) (Table 2). In summer, a positive bias of +6.2 % is calculated for the whole European domain, with the bias being +4.4 % over land and +9.4 % over ocean. As seen in Table 2, the bias is positive for

all the sub-regions, ranging from +2.3 % (EE) to +10.4 % (CM), except for NE (−9.4 %). RegCM4 clearly overestimates SSR for latitudes less than ∼ 55° N and underestimates SSR for higher latitudes (Fig. 2c). For the whole European domain, NME is 11.1 % (10.7 % over land and 11.9 % over ocean), ranging from 8.9 % (EM, IP) to 13.8 % (NE) (Table 2). A positive bias of +2.4 % is found for Europe in autumn, with the corresponding values being −0.9 % over land-covered and +8.4 % over ocean-covered regions. EE (−9.8 %) and CE (−7.2 %) are the regions with the strongest negative bias, while the regions with the strongest positive bias are the ones to the south, namely NA (+5.5 %), CM (+5.3 %) and EM (+5.0) (see also Table 2). This is also seen in Fig. 2d, where RegCM4 overestimates SSR for latitudes less than ∼ 42° N. NME is 11.3 % for the whole European domain, being 11.0 % over land and 11.8 % over ocean. NME ranges from 8.1 % (NA) to 22.1 % (NE) (Table 2).

The seasonal variability in RegCM4 SSR, CM SAF SSR and their difference, for the whole European domain, for the land- and ocean-covered part of Europe, and for the seven sub-regions of interest, is presented in Fig. 3a–j. For Europe as a whole, the largest difference between RegCM4 and CM SAF SSR is observed in summer, with July being the month with the highest RegCM4–CM SAF difference (20.3 W m^{-2}). Over land, the difference between RegCM4 and CM SAF SSR is nearly zero for winter and autumn months. During spring, in March and April, RegCM4 underestimates SSR, while in summer SSR is overestimated, especially in July. However, over ocean, SSR is overestimated by RegCM4 in all months. The highest RegCM4–CM SAF differences are observed during the warm period (May–September). Over NE, RegCM4 underestimates SSR for the months from March to September and overestimates SSR during the winter months. The seasonal variability in the difference between RegCM4 and CM SAF is pretty similar over CE and EE. The simulations underestimate SSR in spring (especially during April) and autumn and overestimate SSR in summer. Over IP, SSR is overestimated again in May and during the summer and underestimated in February, March, November and December. For CM and EM, the seasonal variability in the difference between RegCM4 and CM SAF is almost identical. RegCM4 significantly overestimates SSR from April to October, while for the rest of the months the difference is nearly zero. Finally, over NA, the seasonal variability in the difference is close to the one appearing over CM and EM, but here SSR is also overestimated by RegCM4 in March.

3.2 Cloud fractional cover

CFC plays a determinant role for the SSR levels. Therefore, we compare the CFC patterns simulated with RegCM4 against CFC patterns from MSG CM SAF for the common period 2004–2009. Overall, CFC is underestimated by RegCM4 over Europe by 24.3 % on an annual basis (13.7 % over land and 38.4 % over ocean) despite the fact that, over specific regions (e.g., within IP and NA), CFC is overestimated (see Table 3). Underestimation is observed for all seasons, NA being the only region with a bias of +8.1 % in winter and a bias of +13.1 % in autumn (see Table S3). As shown in Fig. 4a–d, the underestimation of CFC from RegCM4 is stronger over ocean, especially in summer, while strong overestimation is observed over regions in western NA in winter and spring, eastern NA in summer, and the whole of NA during autumn. The latitudinal variability in RegCM4 CFC, CM SAF CFC and their difference is presented in Fig. 5. A clear, strong underestimation of CFC from RegCM4 is observed for all the latitudinal bands and seasons apart from latitudes around 30° N, where CFC is slightly overestimated in autumn. The seasonal variability in RegCM4 CFC, CM SAF CFC and their difference, for the whole European domain, for the land- and ocean-covered part of Europe, and for the seven sub-regions of interest, is presented in Fig. 6a–j. CFC is underestimated steadily by RegCM4 throughout a year, with the underestimation being much stronger over the ocean than over land (see Fig. 6b and c). This underestimation is observed for all the sub-regions except for NA, where CFC is underestimated from April to September and overestimated for the rest of the months.

Generally, lower CFCs would lead to higher SSR levels. However, a comparison of the SSR bias patterns appearing in Fig. 1a–d with the CFC bias patterns appearing in Fig. 4a–d, as well as the biases appearing in Table 1 and Table S3 and the differences and other metrics appearing in Table S2 and Table S4, reveals that, for some areas and seasons, the RegCM4–CM SAF SSR deviations cannot be explained through the corresponding CFC deviations (e.g., land-covered regions during spring and autumn). This is in line with the findings of Katragkou et al. (2015), where the WRF–ISCCP SSR deviations could not always be attributed

Table 3. Annual normalized mean bias (NMB) of RegCM4–CM SAF CFC, COT, Rel and Rei; RegCM4–MACv1 ASY and SSA; RegCM4–CERES ALB; and RegCM4–ERA-Interim WV. When the difference between RegCM4 and CM SAF or CERES or ERA-Interim is statistically significant at the 95 % confidence level due to a two-independent-sample *t* test, the NMB values are marked with bold letters, while in the opposite case they are marked with an asterisk. Positive NMBs are italic, while negative NMBs are underlined.

	CFC	COT	Rel	Rei	AOD	ASY	SSA	ALB	WV
EU	**–24.3**	***4.3***	**–36.1**	**–28.3**	**–35.3**	**–1.1**	**–4.2**	***1.6***	***12.0***
LA	**–13.7**	***7.3***	**–47.7**	**–26.4**	**–32.1**	**–1.8**	**–4.3**	**–28.3**	***11.4***
OC	**–38.4**	**–2.5**	**–18.3**	**–31.1**	**–42.0**	***0.1***	**–4.1**	***131.1***	***12.8***
NE	**–20.3**	***54.3***	**–32.8**	**–31.3**	**–75.9**	***1.0***	**–5.6**	***5.2***	***13.1***
CE	**–19.7**	***24.1***	**–45.1**	**–24.0**	**–63.6**	*0.0**	**–5.9**	**–22.7**	***14.0***
EE	**–16.0**	***30.9***	**–44.6**	**–24.2**	**–64.6**	***2.1***	**–3.5**	**–40.7**	***10.8***
IP	**–13.7**	**–13.9**	**–46.1**	**–27.3**	**–7.4**	**–1.5**	**–4.8**	**–3.8**	***14.4***
CM	**–31.2**	**–30.7**	**–26.7**	**–27.6**	**–19.3**	**–0.7**	**–3.5**	***85.9***	***10.4***
EM	**–28.8**	**–22.0**	**–29.3**	**–28.4**	**–34.2**	**–0.0**	**–2.3**	***35.4***	***10.9***
NA	*0.4**	**–39.8**	**–47.3**	**–30.0**	***25.0***	**–7.9**	**–3.5**	**–26.4**	***8.7***

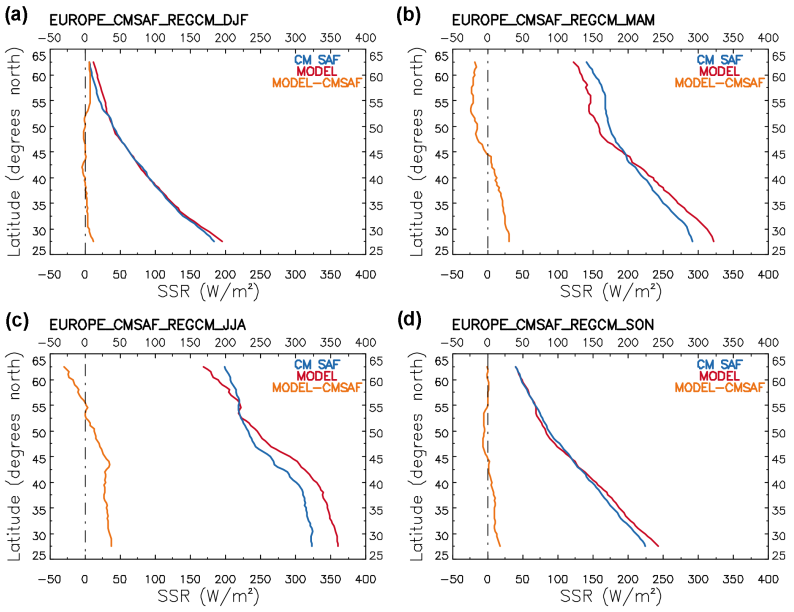

Figure 2. Latitudinal variability in RegCM4 SSR (red), CM SAF SSR (blue) and their difference (orange) over Europe for **(a)** winter (DJF), **(b)** spring (MAM), **(c)** summer (JJA) and **(d)** autumn (SON) from MSG SEVIRI observations.

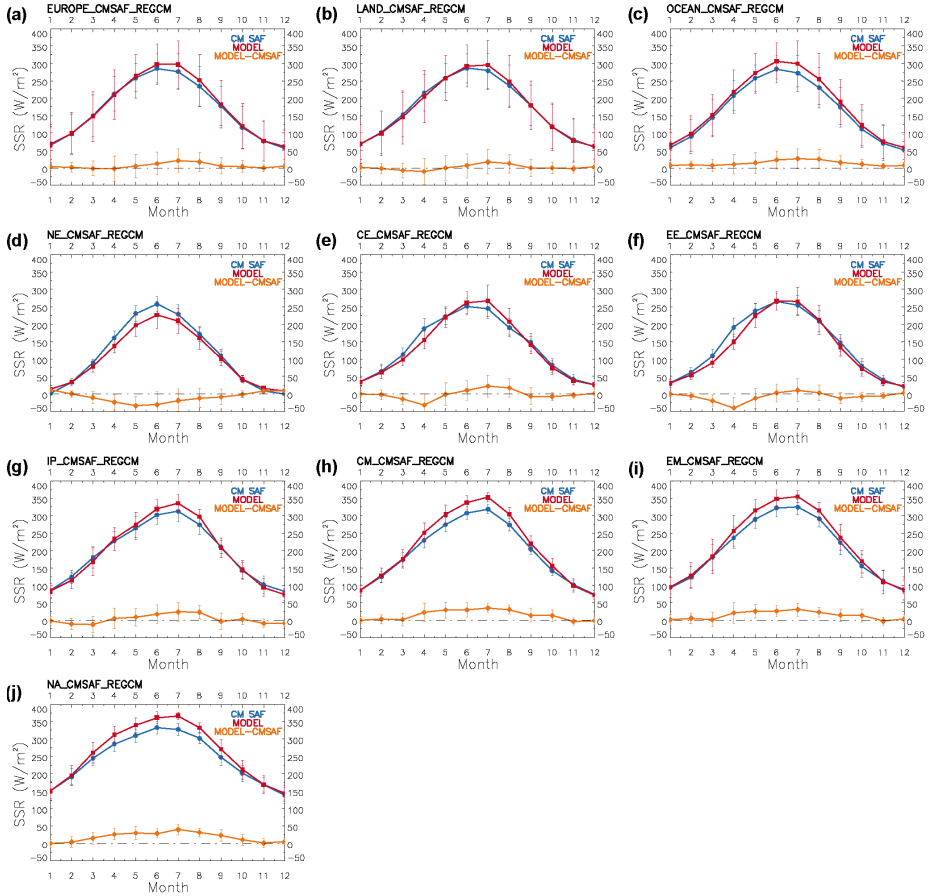

Figure 3. Seasonal variability in RegCM4 SSR (red), CM SAF SSR (blue) and their difference (orange) over **(a)** the whole of Europe, **(b)** land, **(c)** ocean, **(d)** NE, **(e)** CE, **(f)** EE, **(g)** IP, **(h)** CM, **(i)** EM, and **(j)** NA from MSG SEVIRI observations.

to CFC deviations. As discussed there, the role of microphysical cloud properties should also be taken into account. Following this, in the next paragraph we go a step further, taking into account the effect of COT.

3.3 Cloud microphysical properties

3.3.1 Cloud optical thickness

COT is a measure of the transparency of clouds and, along with CFC, determines the transmission of shortwave radiation through clouds (Gupta et al., 1993). In this paragraph, the RegCM4 COT patterns are compared against COT patterns from MSG CM SAF for the common period 2004–2009. Overall, COT is overestimated by RegCM4 over Europe by 4.3 % on an annual basis, the bias being positive over land (+7.3 %) but negative over ocean (−2.5 %) (see Table 3). In addition, COT bias varies with seasons, being positive in spring and autumn and negative in winter and summer (see Tables S5 and S6). As shown in Fig. 7a–d, positive biases are mostly observed over land-covered regions of CE, EE and NE and negative biases over NA and the regions around the Mediterranean Sea. In fact, there is a strong latitudinal variability in the RegCM4–CM SAF COT difference for all the seasons as presented in Fig. 8a–d. RegCM4 underestimates COT for latitudes below $\sim 45°$ N in winter, spring and autumn and for latitudes below $\sim 50°$ N in summer. The seasonal variability in RegCM4 COT, CM SAF COT and their difference for the whole European domain, for the land- and ocean-covered part of Europe, and for the seven sub-regions of interest, is presented in Fig. 9a–j. In general, the RegCM4–CM SAF COT difference is not steadily positive or negative but varies from month to month over both land and ocean. RegCM4 steadily overestimates COT throughout a year only over NE and underestimates COT over CM and NA. It needs to be mentioned that there are no COT retrievals over NE for December and January due to limited illumination at those latitudes during this period of the year. This is also the reason for there being missing grid cells in the top-right corner of Fig. 7a–d.

A comparison of the SSR bias patterns appearing in Fig. 1a–d with the CFC (Fig. 4a–d) and the COT (Fig. 7a–d) bias patterns reveals that COT could explain part of the RegCM4–CM SAF SSR deviations that could not be explained through CFC (e.g., NE, CE, EE). The same conclusions can be reached by comparing the seasonal variability in SSR, CFC and COT over the region of interest (see Figs. 3, 6 and 9). However, other parameters are expected to be responsible for the remaining unexplained RegCM4–CM SAF SSR deviation.

3.3.2 Cloud effective radius

Re is a microphysical optical property expressing the size of cloud droplets in the case of liquid clouds and the size of ice crystals in the case of ice clouds. Re of liquid (Rel) and ice (Rei) clouds plays a critical role in the calculation of the optical thickness of clouds as well as their albedo (see Eqs. 4–7 in Sect. 2.1). The evaluation of RegCM4 Rel and Rei against observational data from CM SAF reveals a significant underestimation over the whole European domain (bias of −36.1 % for Rel and −28.3 % for Rei) (see Tables 3, S7 and S8). This is also apparent in the maps appearing in Figs. S6 and S8. In the case of ice clouds, the biases over land and ocean do not differ significantly. However, for liquid clouds, the bias over land is more than double the bias over ocean (see Tables 3, S7 and S8). This is due to the very low RegCM4 Rel values appearing over land, while the CM SAF data set does not exhibit such a land–ocean difference. A possible explanation for this could be the fact that a different approach is used over land (constant Rel of 10 µm) and ocean (Eq. 1) for liquid clouds, while for ice clouds the parameterization is the same for land and ocean (Eq. 2). The fact that the average Rel value over land (5.65 ± 1.06 µm) is very close to the lowest Rel boundary (5 µm) according to Eq. (1) possibly points towards an underestimation of the liquid cloud height and vertical development. Also, this Rel land–ocean difference is responsible for the COT land–ocean difference (see Table 3) according to Eq. (4). In general, the underestimation of Re would result in more reflective clouds and hence in underestimated SSR levels. It should be mentioned here that the latitudinal and monthly variability in RegCM4 Rel and Rei as well as CM SAF Rel and Rei and their difference, for the whole European domain, for the land- and ocean-covered part of Europe, and for the seven sub-regions, is presented in the Supplement of this paper (Figs. S6 to S9). A constant underestimation of Rel and Rei is observed for the whole of Europe.

3.4 Aerosol optical properties

As discussed in Sect. 2.4, AOD along with CFC and COT constitute the major controllers of SSR. A comparison of the RegCM4 AOD_{550} seasonal patterns with climatological AOD_{550} values from MACv1 is presented in Fig. S10a–d. On an annual basis, RegCM4 overestimates AOD over the region of NA (bias of +25.0 %) (see Table 3). The overestimation is very strong during winter and much weaker in spring and autumn (see Tables S9 and S10). This overestimation over regions affected by dust emission has been discussed comprehensively in Nabat et al. (2012) and has to do with the dust particle size distribution schemes utilized by RegCM4 (Alfaro and Gomes, 2001; Kok, 2011). Nabat et al. (2012) showed that the implementation of the Kok (2011) scheme generally reduces the dust AOD overestimation in RegCM4 over the Mediterranean Basin. However, a first climatological comparison of RegCM4 dust AODs with data from CALIOP/CALIPSO (A. Tsikerdekis, personal communication, 2015) has shown that both schemes overestimate dust AOD over Europe, and therefore the se-

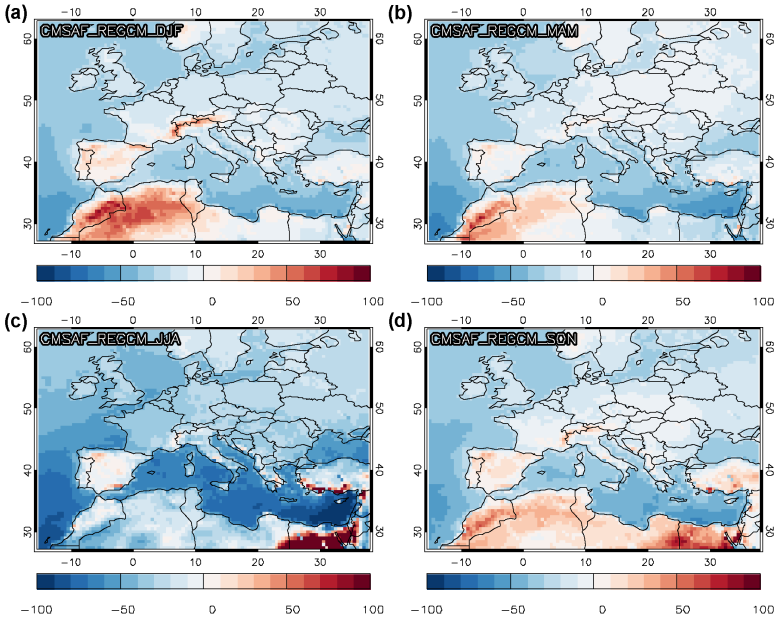

Figure 4. The same as Fig. 1 but for RegCM4 and CM SAF CFC.

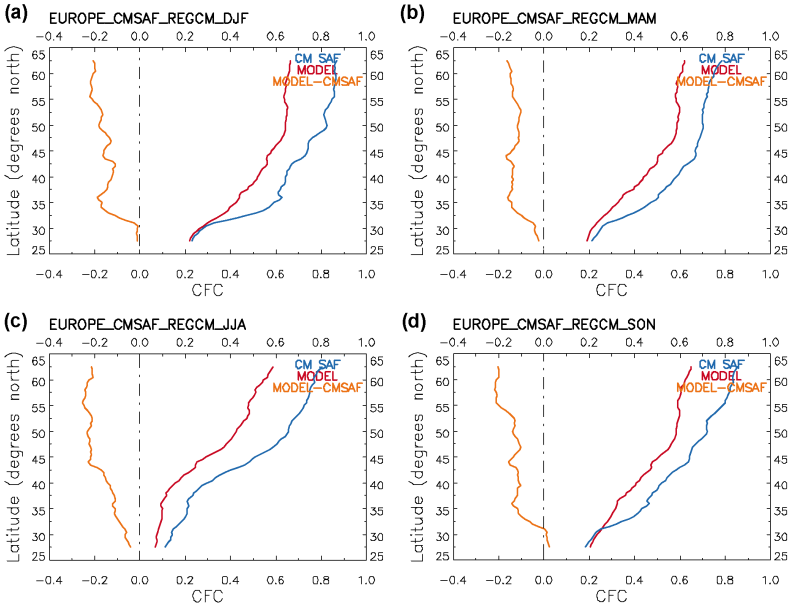

Figure 5. The same as Fig. 2 but for RegCM4 and CM SAF CFC.

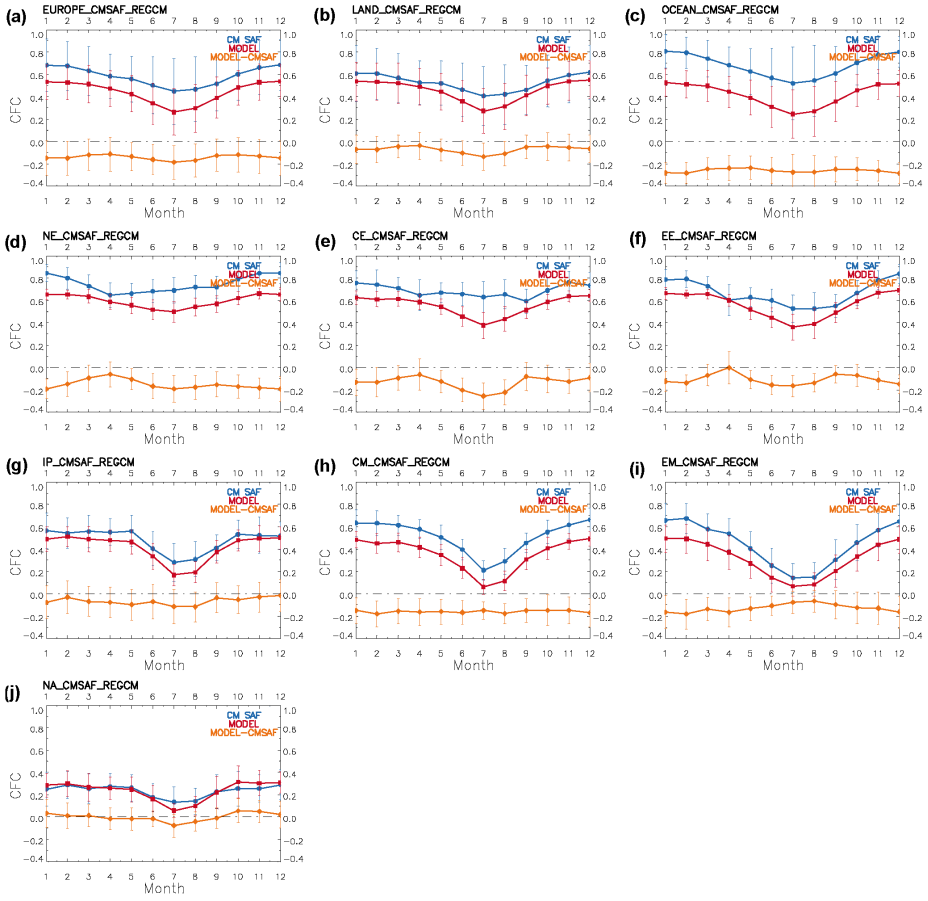

Figure 6. The same as Fig. 3 but for RegCM4 and CM SAF CFC.

lection of a specific dust scheme is not expected to drastically change our results. However, AOD is significantly underestimated over the rest of the domain. This should be expected as RegCM does not account for several types of aerosols, both anthropogenic (e.g., nitrates, ammonium and secondary organic aerosols, industrial dust) and natural (e.g., biogenic aerosols), which potentially play an important role (Kanakidou et al., 2005; Zanis et al., 2012). This overestimation/underestimation dipole in winter, spring and autumn is also reflected in Fig. S11. RegCM4 overestimates AOD for latitudes below $\sim 40^\circ$ N in winter, for latitudes below $\sim 35^\circ$ N in spring, and for a narrow latitudinal band (~ 30–33° N) in autumn. In summer, RegCM4 steadily underestimates AOD compared to MACv1. The seasonal variability in RegCM4 AOD_{550}, MACv1 AOD_{550} and their difference, for the whole European domain, for the land- and ocean-covered part of Europe, and for the seven sub-regions of interest, is presented in Fig. S12a–j. In general, RegCM4 clearly underestimates AOD throughout a year over regions that are not affected heavily by Sahara dust transport. This underestimation would cause an overestimation of SSR if all the other parameters were kept constant. The opposite is true for the region of NA, where AOD, except for summer, is significantly overestimated.

As in the case of COT and Re, in order to fully assess the contribution of aerosols to the observed RegCM4–CM SAF SSR deviations, one has to take into account ASY and SSA besides AOD. A comparison of RegCM4 ASY with climatological values from MACv1 reveals a small underestimation from RegCM4 over Europe (bias of $-1.1\,\%$) (Tables 3 and S11). As shown in Fig. S13, RegCM4 underestimates ASY for latitudes below $\sim 40^\circ$ N and slightly overestimates ASY for the rest of the region. Except for NA, where RegCM4 underestimates ASY throughout the year, RegCM4 slightly overestimates ASY for the warm period over NE, CE and EE, while for the rest of the sub-regions the RegCM4–MACv1 difference is close to zero (see Fig. S14). In contrast to the case of ASY, RegCM4 steadily underestimates SSA compared to MACv1 over Europe by 4.2 % (see Tables 3 and S12 and Fig. S15). Moreover, as shown in Fig. S16, SSA is underestimated on an annual basis for the total of the subregions.

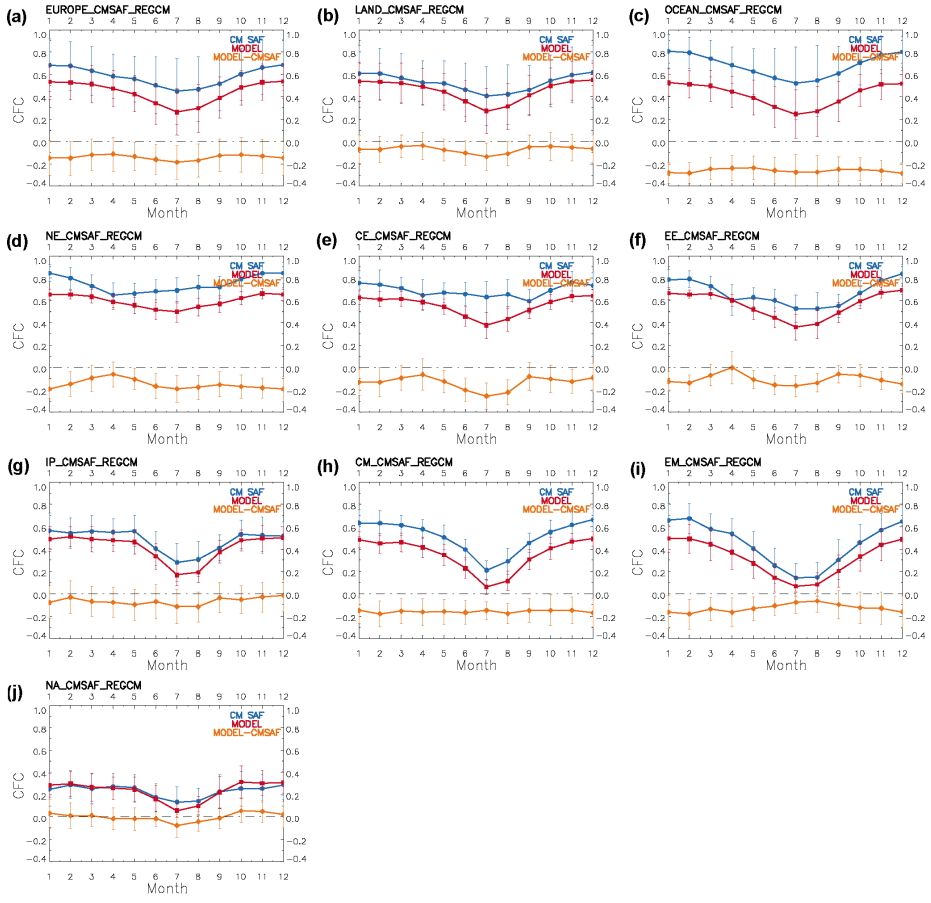

Figure 7. The same as Fig. 1 but for RegCM4 and CM SAF COT.

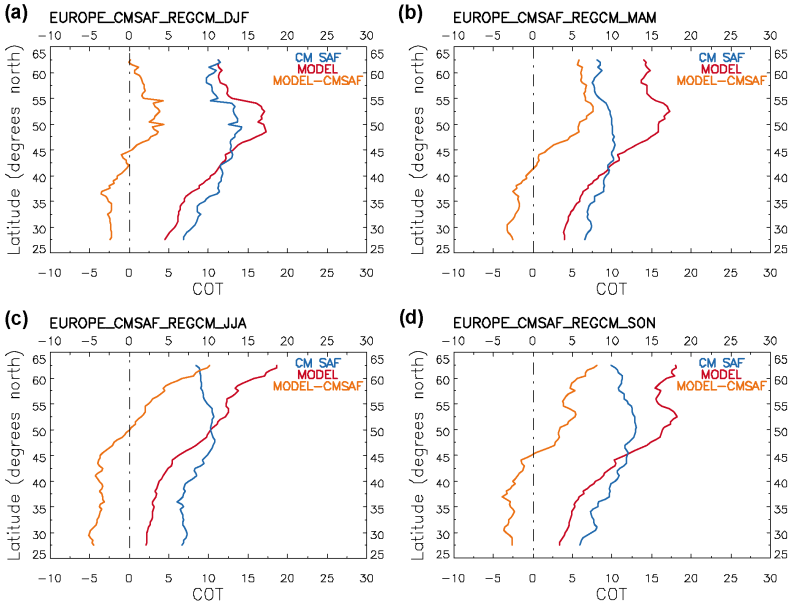

Figure 8. The same as Fig. 2 but for RegCM4 and CM SAF COT.

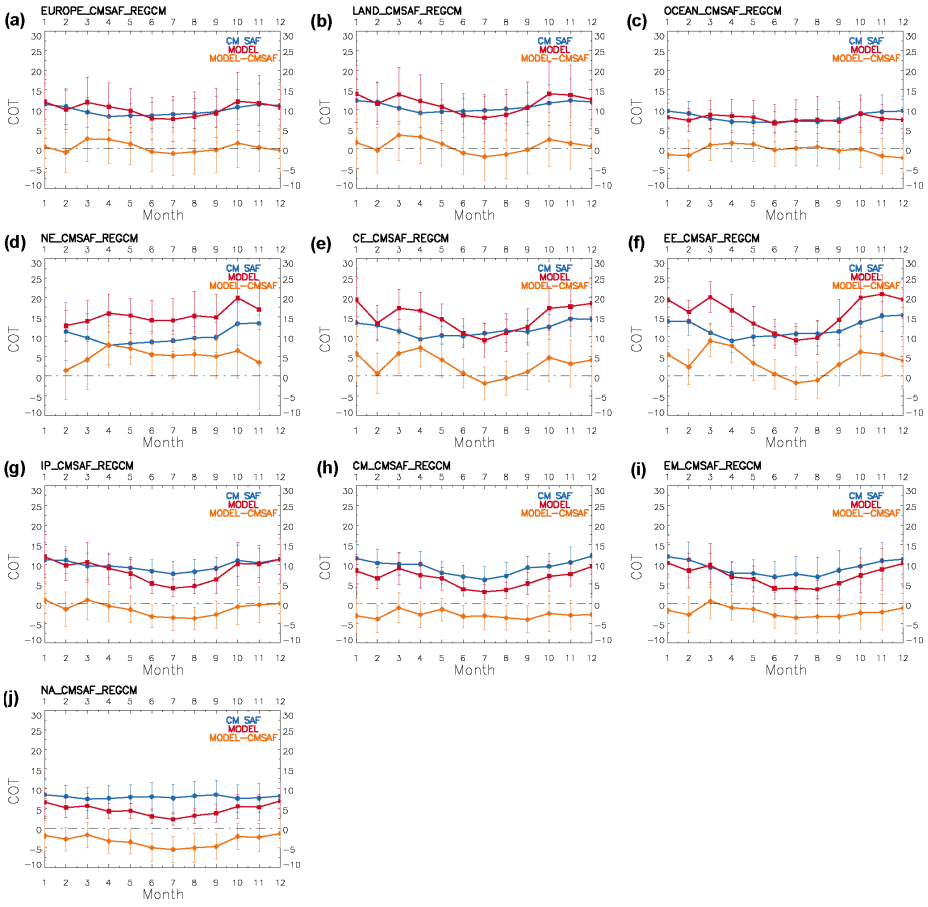

Figure 9. The same as Fig. 3 but for RegCM4 and CM SAF COT.

3.5 Other parameters

Apart from the major (CFC, COT, AOD) and minor (Re, ASY, SSA) SSR determinants, which are discussed above in detail, there are also a number of other parameters that could impact the simulation skills of RegCM4 compared to CM SAF, since these parameters are used as input within the radiative scheme of the model.

As previously discussed, WV is another parameter that affects the transmission of solar radiation within the atmosphere. RegCM4 is found here to overestimate WV compared to ERA-Interim reanalysis all over Europe with a bias of $\sim 12\,\%$ (see Tables 3 and S13). This becomes more than obvious when looking at the bias map and the seasonal and latitudinal variability in the two data sets (see Figs. S17 and S18).

In line with the study of Güttler et al. (2014), RegCM4 exhibits a significant underestimation of ALB over CE, EE and NA (see Table 3) compared to climatological data from CERES (see Sect. 2.3). In general, there is a striking difference between land- and ocean-covered regions (Figs. S19 and S20). Over land RegCM4 underestimates ALB by 28.3 %, while over ocean ALB is strongly overestimated by 131 %. As previously mentioned, the comparisons of RegCM4 with non-observational data presented in this paragraph do not constitute an evaluation of RegCM4. However, these comparisons give us an insight into how several parameters affect the ability of RegCM4 to simulate SSR.

3.6 Assessing the effect of various parameters on RegCM's SSR

As discussed in detail in Sect. 2.4, the potential contribution of each one of the aforementioned parameters in the deviation between RegCM4 and CM SAF SSR is assessed quantitatively with the use of the SBDART radiative transfer model. The results of this analysis are presented in Fig. 10. The percent contribution of each parameter to the RegCM4–CM SAF SSR difference is calculated on a monthly basis. Results for NE are not included in this paper, since COT and Re are not available from CM SAF during winter (December, January) and also due to the low insolation levels for several months at high latitudes. Results for NA are also not presented. This region is characterized by a significant day-to-day variability in cloudiness and aerosols and therefore the statistical significance of a monthly analysis like the one

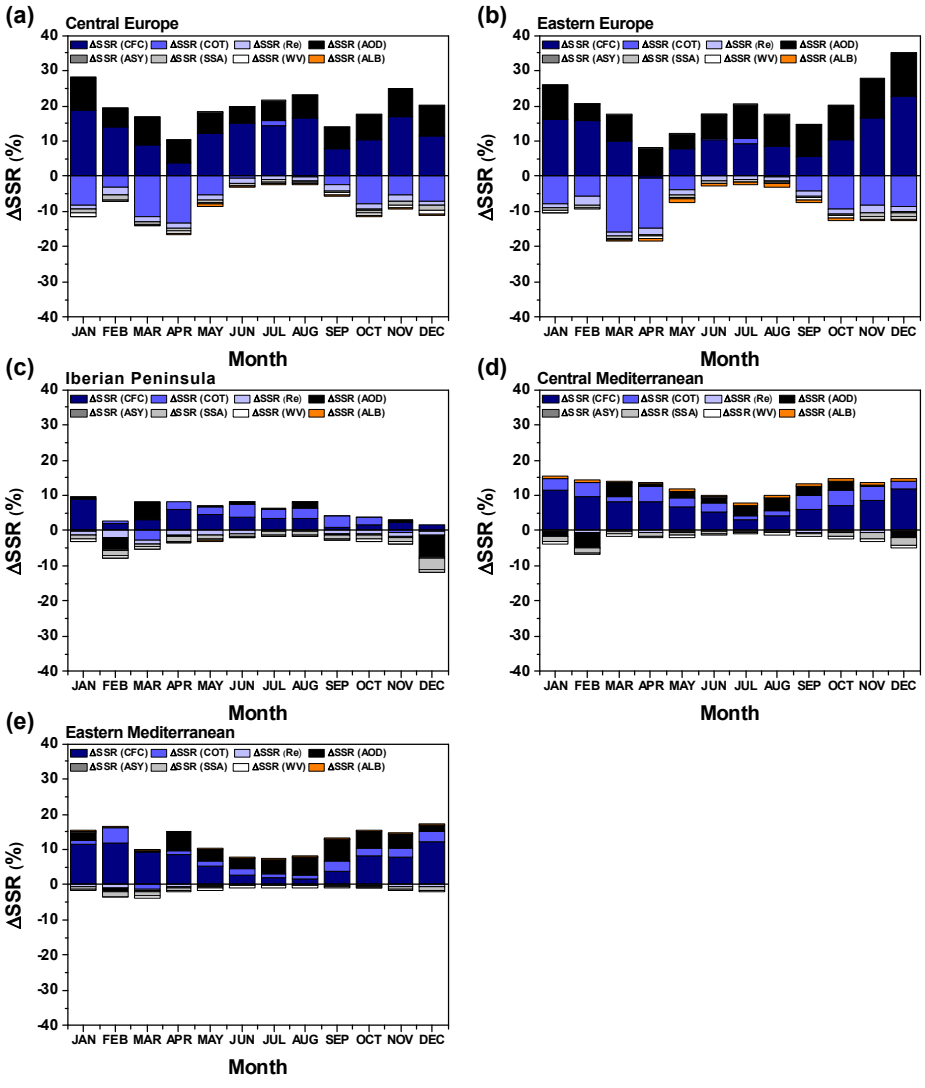

Figure 10. ΔSSR (%) caused by CFC, COT, Re, AOD, ASY, SSA, WV and ALB for **(a)** CE, **(b)** EE, **(c)** IP, **(d)** CM and **(e)** EM.

presented here would be limited. Another source of uncertainty would be the use of spatial averages within the radiative transfer simulations, since the western and eastern part of the region differ significantly by means of aerosol load and cloud coverage and hence the region cannot be considered homogeneous.

It should be mentioned that the potential percent contributions to the RegCM4–CM SAF SSR difference presented in Fig. 10 do not include the relative contribution due to algorithmic issues of the CM SAF product used here and also uncertainties introduced by the method itself (e.g., SBDART simulation accuracy, use of monthly data, spatial averaging). Therefore the contributions appearing in Fig. 10 are not directly connected to the RegCM4–CM SAF differences presented in Fig. 3. In fact, part of these differences is due to the overestimation of SSR by CM SAF due to the method used for the production of the data set. Hence, the ΔSSR values presented below do not include the bias introduced by the CM SAF algorithm. As mentioned in Sect. 2.2, CM SAF was found to overestimate SSR compared to ground observations over Europe by 5.2 $\mathrm{W\,m^{-2}}$ for the 1983–2005 MFG period (Sanchez-Lorenzo et al., 2013) and by 3.16 $\mathrm{W\,m^{-2}}$ for the 1983–2010 MFG–MSG period (Posselt et al., 2014). Following these studies, the CM SAF MSG data (2006–2009) used in this work are validated using ground-based observations from 26 stations (23 stations from the World Radiation Data Center (WRDC) and 3 independent stations) evenly distributed around Europe (see Fig. S21). Overall, it is found that CM SAF overestimates SSR on an annual basis by 4.5 $\mathrm{W\,m^{-2}}$ over CE, 8.8 $\mathrm{W\,m^{-2}}$ over EE, 2.4 $\mathrm{W\,m^{-2}}$ over IP, 7.8 $\mathrm{W\,m^{-2}}$ over CM and 4.5 $\mathrm{W\,m^{-2}}$ over EM, the overestimation being much higher during the warm period (Fig. S22).

As seen in Fig. 10a, apart from the bias introduced by the CM SAF retrieval methodology, the percent RegCM4–CM SAF SSR difference (ΔSSR) over CE is mostly determined by CFC, COT and AOD. However, for specific months, Re and the other parameters also play an important role, leading to an underestimation of SSR. CFC leads to a significant overestimation of SSR on an annual basis ranging from 3.7 % (April) to 18.6 % (January). Apart from in July, COT leads to an underestimation of SSR, April being the month with the highest underestimation (ΔSSR of −13.3 %). AOD, on the other hand, leads to an overestimation of SSR over CE ranging from +4.6 % (June) to +9.5 % (January). As mentioned in Sect. 2.4, the procedure was repeated assuming the simulated SSR fields with all the CM SAF, MACv1 and ERA-Interim input data as the control run and replacing each time the corresponding parameter with data from RegCM4. The results from this repetition were similar to the results presented above, showing that the effect of the interdependence of the parameters investigated here is low and does not affect the validity of our results. The same holds for all the subregions. The results from the inverse procedure and the differences to the results presented here are given in Figs. S23 and S24, respectively.

In line with CE, ΔSSR over EE is mostly determined by CFC, COT and AOD (Fig. 10b). Apart from in April, CFC leads to an overestimation of SSR, December being the month with the highest overestimation (+22.9 %). Apart from in June and July, COT causes an underestimation of SSR, March/August being the month with the highest/lowest underestimation (−15.8/−0.2 %). On the other hand, AOD leads to an overestimation of SSR the whole year, December/May being the month with the highest/lowest overestimation (+12.3/+4.2 %). Re also plays a role, leading to an underestimation of SSR, which ranges from −1.06 % (July) to −2.5 % (February). All the other parameters play a minor role, generally leading to an underestimation of SSR.

Over IP, despite the fact that the dominant parameters are CFC and COT, for some months AOD, SSA and Re contribute substantially to ΔSSR (Fig. 10c). CFC leads to an overestimation of SSR, January/September being the month with the highest/lowest overestimation of SSR (+9.1/+1.1 %). COT causes an important overestimation of SSR from April to October (e.g., +3.7 % in June) and a significant underestimation during March (−2.8 %). On the other hand, Re leads to an underestimation of SSR that ranges from −1.3 % in April to −0.3 % in August. The same holds for SSA, with an average annual SSR underestimation of −1.2 %, while AOD exhibits a mixed behavior leading to either underestimation (a maximum of −6.1 % in December) or overestimation (a maximum of +4.9 % in March).

As seen in Fig. 10d, ΔSSR over CM is mostly determined by CFC, COT, AOD and SSA. CFC causes a significant overestimation of SSR ranging from +3.2 % (July) to +11.9 % (December). COT leads to an overestimation of SSR on an annual basis, October being the month with the highest overestimation (+4.6 %). AOD causes an overestimation of SSR over CM for the period from March to October (average ΔSSR of +2.2 %) and an underestimation during winter (average ΔSSR of −2.3 %). SSA, on the other hand, causes an underestimation of SSR on an annual basis ranging from −0.5 % (July) to −1.9 % (December).

ΔSSR over EM is dominated by the relative contribution of CFC, AOD and COT (see Fig. 10e). CFC causes an overestimation of SSR on an annual basis ranging from +1.7 % (August) to +12.2 % (December). Apart from in February, AOD causes a significant overestimation ranging from +0.5 % (March) to +6.0 % (September). Apart from in March, COT leads to an overestimation of SSR, February being the month with the highest overestimation (+4.3 %). SSA also plays a role, in some cases comparable in magnitude to that of COT or AOD (e.g., January, March).

In summary, for the total of the five sub-regions, CFC, COT and AOD are the most important factors that determine the SSR deviations between RegCM4 and CM SAF on an annual basis. The underestimations/overestimations of CFC, COT and AOD by the model cause an annual absolute deviation of the SSR compared to CM SAF of 8.4, 3.8 and 4.5 %, respectively.

4 Conclusions

In the present study, a decadal simulation (2000–2009) with the regional climate model RegCM4 is implemented in order to assess the model's ability to represent the SSR patterns over Europe. The RegCM4 SSR fields are evaluated against satellite-based observations from CM SAF. The annual bias patterns of RegCM4–CM SAF are similar for both MFG (2000–2005) and MSG (2006–2009) observations. The model slightly overestimates SSR compared to CM SAF over Europe, the bias being +1.5 % for MFG and +3.3 % for MSG observations. Moreover, the bias is much lower over land than over ocean, while some differences appear locally between the seasonal and annual bias patterns.

In order to understand the RegCM4–CM SAF SSR deviations, CFC, COT and Re data from RegCM4 are compared against observations from CM SAF (MSG period). For the same reason, AOD, ASY, SSA, WV and ALB from RegCM4 are compared against data from MACv1, ERA-Interim reanalysis and CERES since these data are similar to the ones used as input in the retrieval of CM SAF SSR.

CFC is significantly underestimated by RegCM4 compared to CM SAF over Europe by 24.3 % on an annual basis. Part of the bias between RegCM4 and CM SAF SSR can be explained through CFC, with the underestimation of CFC leading to a clear overestimation of SSR. It was also found that RegCM4 overestimates COT compared to CM SAF on an annual basis, suggesting that COT may explain part of the RegCM4–CM SAF SSR deviations that could not be explained through CFC over specific regions. In addi-

tion, RegCM4 significantly underestimates Rel and Rei compared to CM SAF over the whole European domain on an annual basis. A comparison of the RegCM4 AOD seasonal patterns with AOD values from the MACv1 aerosol climatology reveals that RegCM4 overestimates AOD over the region of NA and underestimates it for the rest of the European domain. ASY and SSA are slightly underestimated by the model. The comparison of RegCM4 WV against data from ERA-Interim reanalysis reveals a clear overestimation over Europe. In line with previous studies, RegCM4 significantly underestimates ALB over CE, EE and NA compared to climatological data from CERES, with a striking difference between land and ocean.

The combined use of SBDART radiative transfer model with RegCM4, CM SAF, MACv1, CERES and ERA-Interim data for the common period 2006–2009 shows that the difference between RegCM4 and CM SAF SSR, apart from the bias introduced by the CM SAF algorithm, is mostly explained through CFC, COT and AOD deviations. In the majority of the regions, CFC leads to an overestimation of SSR by RegCM4. In some cases, COT leads to a significant underestimation of SSR by RegCM4, while for the majority of the regions it leads to an overestimation. AOD is generally responsible for the overestimation of SSR. The other parameters (Re, ASY, SSA, WV and ALB) play a less significant role in the RegCM4–CM SAF SSR deviations. Overall, CFC, COT and AOD are the major determinants of the SSR differences between RegCM4 and CM SAF, causing an absolute deviation on an annual basis of 8.4, 3.8 and 4.5 %, respectively. These results highlight the importance of other parameters apart from CFC, which has been examined in previous model evaluation studies (e.g., Jaeger et al., 2008; Markovic et al., 2008; Kothe and Ahrens, 2010; Kothe et al., 2011, 2014; Güttler et al., 2014).

Overall, it is shown in this study that RegCM4 adequately simulates the SSR patterns over Europe. However, it is also shown that the model significantly over- or underestimates several parameters that determine the transmission of solar radiation in the atmosphere. The good agreement between RegCM4 and satellite-based SSR observations from CM SAF is to a great extent a result of the conflicting effect of these parameters. Our results suggest that there should be a reassessment of the way these parameters are represented within the model so that SSR is well simulated, but also for the right reasons. This would also allow for a safer investigation of the dimming/brightening effect since the SSR deviations would be safely dedicated to one or the other parameter. It is suggested here that a similar approach should be implemented in the future in the same or other regional climate models, with various setups also utilizing new satellite products (e.g., CM SAF SARAH).

The Supplement related to this article is available online at doi:10.5194/acp-15-13195-2015-supplement.

Acknowledgements. This research received funding from the European Social Fund (ESF) and national resources under the operational program Education and Lifelong Learning (EdLL) within the framework of the Action "Supporting Postdoctoral Researchers" (QUADIEEMS project), from EPAN II and PEP under the national action "Bilateral, multilateral and regional R&T cooperations" (AEROVIS Sino-Greek project), and from the European Research Council under the European Union's Seventh Framework Programme (FP7/2007–2013)/ERC grant agreement no. 226144 (C8 project). The authors acknowledge the provision of satellite data by EUMETSAT through the Satellite Application Facility on Climate Monitoring (CM SAF) (www.cmsaf.eu) and the use of MACv1 aerosol climatology data (ftp://ftp-projects.zmaw.de). Special thanks are expressed to ECMWF (www.ecmwf.int) for the provision of ERA-Interim reanalysis data, NASA Langley Research Center for making CERES data available via the CERES ordering tool (http://ceres.larc.nasa.gov), the World Radiation Data Center (WRDC) for making available ground-based surface radiation data (http://wrdc.mgo.rssi.ru), and IESRD/NOA and HCMR for the provision of surface radiation data from the station of Athens and Herakleion, Greece.

Edited by: S. Kazadzis

References

Alfaro, S. C. and Gomes, L.: Modeling mineral aerosol production by wind erosion: emission intensities and aerosol size distribution in source areas, J. Geophys. Res., 106, 18075–18084, doi:10.1029/2000JD900339, 2001.

Allen, M. R. and Ingram, W. G.: Constraints on future changes in climate and the hydrologic cycle, Nature, 419, 224–232, 2002.

Beyer, H. G., Costanzo, C., and Heinemann, D.: Modifications of the Heliosat procedure for irradiance estimates from satellite images, Sol. Energy, 56, 207–212, doi:10.1016/0038-092X(95)00092-6, 1996.

Bodas-Salcedo, A., Williams, K. D., Ringer, M. A., Beau, I., Cole, J. N. S., Dufresne, J.-L., Koshiro, T., Stevens, B., Wang, Z., and Yokohata, T.: Origins of the solar radiation biases over the Southern Ocean in CFMIP2 models, J. Climate, 27, 41–56, doi:10.1175/JCLI-D-13-00169.1, 2014.

Briegleb, B. P.: Delta-Eddington approximation for solar radiation in the NCAR Community Climate Model, J. Geophys. Res., 97, 7603–7612, doi:10.1029/92JD00291, 1992.

Cano, D., Monget, J., Albuisson, M., Guillard, H., Regas, N., and Wald, L.: A method for the determination of the global solar radiation from meteorological satellite data, Sol. Energy, 37, 31–39, doi:10.1016/0038-092X(86)90104-0, 1986.

Chiacchio, M., Solmon, F., Giorgi, F., Stackhouse, P., and Wild, M.: Evaluation of the radiation budget with a regional climate model over Europe and inspection of dimming and brightening, J. Geophys. Res., 120, 1951–1971, doi:10.1002/2014JD022497, 2015.

Collins, W. D., Bitz, C. M., Blackmon, M. L., Bonan, G. B., Bretherton, C. S., Carton, J. A., Chang, P., Doney, S. C., Hack, J. J., Henderson, T. B., Kiehl, J. T., Large, W. G., McKenna, D. S., Santer, B. D., and Smith, R. D.: The Community Climate System Model version 3 (CCSM3), J. Climate, 19, 2122–2143, doi:10.1175/JCLI3761.1, 2006.

Cros, S., Albuisson, M., and Wald, L.: Simulating Meteosat-7 broadband radiances using two visible channels of Meteosat-8, Sol. Energy, 80, 361–367, doi:10.1016/j.solener.2005.01.012, 2006.

Dee, D. P., Uppala, S. M., Simmons, A. J., Berrisford, P., Poli, P., Kobayashi, S., Andrae, U., Balmaseda, M. A., Balsamo, G., Bauer, P., Bechtold, P., Beljaars, A. C. M., van de Berg, L., Bidlot, J., Bormann, N., Delsol, C., Dragani, R., Fuentes, M., Geer, A. J., Haimberger, L., Healy, S. B., Hersbach, H., Hólm, E. V., Isaksen, L., Kållberg, P., Köhler, M., Matricardi, M., McNally, A. P., Monge-Sanz, B. M., Morcrette, J.-J., Park, B.-K., Peubey, C., de Rosnay, P., Tavolato, C., Thépaut, J.-N., and Vitart, F.: The ERA-Interim reanalysis: configuration and performance of the data assimilation system, Q. J. Roy. Meteor. Soc., 137, 553–597, doi:10.1002/qj.828, 2011.

Derrien, M. and Le Gléau, H.: MSG/SEVIRI cloud mask and type from SAFNWC, Int. J. Remote Sens., 26, 4707–4732, 2005.

Dickinson, R. E., Henderson-Sellers, A., and Kennedy, P. J.: Biosphere–atmosphere transfer scheme (bats) version 1e as coupled to the NCAR community climate model, Tech. Rep. NCAR/TN-387+STR, National Center for Atmospheric Research, Boulder, Colorado, USA, 1–72, doi:10.5065/D67W6959, 1993.

Ebert, E. and Curry, J.: A parameterization of ice cloud optical properties for climate models, J. Geophys. Res., 97, 3831–3836, doi:10.1029/91JD02472, 1992.

Emanuel, K. A.: A scheme for representing cumulus convection in large-scale models, J. Atmos. Sci., 48, 2313–2335, 1991.

Emanuel, K. A. and Zivkovic-Rothman, M.: Development and evaluation of a convection scheme for use in climate models, J. Atmos. Sci., 56, 1766–1782, 1999.

Flato, G., Marotzke, J., Abiodun, B., Braconnot, P., Chou, S., Collins, W., Cox, P., Driouech, F., Emori, S., Eyring, V., Forest, C., Gleckler, P., Guilyardi, E., Jakob, C., Kattsov, V., Reason, C., and Rummukainen, M.: Evaluation of climate models, in: Climate Change 2013: The Physical Science Basis. Contribution of Working Group I to the Fifth Assessment Report of the Intergovernmental Panel on Climate Change, edited by: Stocker, T., Qin, D., Plattner, G.-K., Tignor, M., Allen, S., Boschung, J., Nauels, A., Xia, Y., Bex, V., and Midgley, P., chap. 6, 741–866, Cambridge University Press, Cambridge, United Kingdom and New York, NY, USA, 2013.

Giorgi, F., Coppola, E., Solmon, F., Mariotti, L., Sylla, M. B., Bi, X., Elguindi, N., Diro, G. T., Nair, V., Giuliani, G., Cozzini, S., Guettler, I., O'Brien, T. A., Tawfik, A. B., Shalaby, A., Zakey, A. S., Steiner, A. L., Stordal, F., Sloan, L. C., and Brankovic, C.: RegCM4: model description and preliminary tests over multiple CORDEX domains, Clim. Res., 52, 7–29, doi:10.3354/cr01018, 2012.

Grell, G.: Prognostic evaluation of assumptions used by cumulus parameterizations, Mon. Weather Rev., 121, 764–787, 1993.

Grell, G. A., Dudhia, J., and Stauffer, D. R.: Description of the fifth generation Penn State/NCAR Mesoscale Model (MM5), Tech. Rep. NCAR/TN-398+STR, National Center for Atmospheric Research, Boulder, Colorado, USA, 1–121, doi:10.5065/D60Z716B, 1994.

Gu, L., Baldocchi, D., Verma, S., Black, T., Vesala, T., Falge, E., and Dowty, P.: Advantages of diffuse radiation for terrestrial ecosystem productivity, J. Geophys. Res., 107, ACL2.1–ACL2.23, doi:10.1029/2001JD001242, 2002.

Gupta, S. K., Staylor, W. F., Darnell, W. L., Wilber, A. C., and Ritchey, N. A.: Seasonal variation of surface and atmospheric cloud radiative forcing over the globe derived from satellite data, J. Geophys. Res., 98, 20761–20778, doi:10.1029/93JD01533, 1993.

Güttler, I., Brankovic, C., Srnec, L., and Patarcic, M.: The impact of boundary forcing on RegCM4.2 surface energy budget, Climatic Change, 125, 67–78, doi:10.1007/s10584-013-0995-x, 2014.

Hammer, A., Heinemann, D., Hoyer, C. R. K., Lorenz, E., Mueller, R., and Beyer, H.: Solar Energy assessment using remote sensing technologies, Remote Sens. Environ., 86, 423–432, doi:10.1016/S0034-4257(03)00083-X, 2003.

Holtslag, A. A. M., De Bruijn, E. I. F., and Pan, H.-L.: A high resolution air mass transformation model for short-range weather forecasting, Mon. Weather Rev., 118, 1561–1575, 1990.

IPCC: Climate Change 2013: the Physical Science Basis: Summary for Policymakers, Cambridge University Press, Cambridge, UK, New York, NY, USA, 2013.

Jaeger, E. B., Anders, I., Lüthi, D., Rockel, B., Schär, C., and Seneviratne, S. I.: Analysis of ERA40-driven CLM simulations for Europe, Meteorol. Z., 17, 349–367, 2008.

Kanakidou, M., Seinfeld, J. H., Pandis, S. N., Barnes, I., Dentener, F. J., Facchini, M. C., Van Dingenen, R., Ervens, B., Nenes, A., Nielsen, C. J., Swietlicki, E., Putaud, J. P., Balkanski, Y., Fuzzi, S., Horth, J., Moortgat, G. K., Winterhalter, R., Myhre, C. E. L., Tsigaridis, K., Vignati, E., Stephanou, E. G., and Wilson, J.: Organic aerosol and global climate modelling: a review, Atmos. Chem. Phys., 5, 1053–1123, doi:10.5194/acp-5-1053-2005, 2005.

Kato, S., Loeb, N. G., Rose, F. G., Doelling, D. R., Rutan, D. A., Caldwell, T. E., Yu, L., and Weller, R. A.: Surface irradiances consistent with CERES-derived top-of-atmosphere shortwave and longwave irradiances, J. Climate, 26, 2719–2740, doi:10.1175/JCLI-D-12-00436.1, 2013.

Katragkou, E., García-Díez, M., Vautard, R., Sobolowski, S., Zanis, P., Alexandri, G., Cardoso, R. M., Colette, A., Fernandez, J., Gobiet, A., Goergen, K., Karacostas, T., Knist, S., Mayer, S., Soares, P. M. M., Pytharoulis, I., Tegoulias, I., Tsikerdekis, A., and Jacob, D.: Regional climate hindcast simulations within EURO-CORDEX: evaluation of a WRF multi-physics ensemble, Geosci. Model Dev., 8, 603–618, doi:10.5194/gmd-8-603-2015, 2015.

Kawamoto, K. and Hayasaka, T.: Relative contributions to surface shortwave irradiance over China: a new index of potential radiative forcing, Geophys. Res. Lett., 35, L17809, doi:10.1029/2008GL035083, 2008.

Kawamoto, K. and Hayasaka, T.: Geographical features of changes in surface shortwave irradiance in East Asia estimated using the potential radiative forcing index, Atmos. Res., 96, 337–343, doi:10.1016/j.atmosres.2009.09.016, 2010.

Kawamoto, K. and Hayasaka, T.: Cloud and aerosol contributions to variation in shortwave surface irradiance over East Asia in July during 2001 and 2007, J. Quant. Spectrosc. Ra., 112, 329–337, doi:10.1016/j.jqsrt.2010.08.002, 2011.

Kiehl, J. T., Hack, J. J., Bonan, G. B., Boville, B. A., Breigleb, B. P., Williamson, D., and Rasch, P.: Description of the NCAR community climate model (CCM3), Tech. Rep. NCAR/TN-420+STR,

National Center for Atmospheric Research, Boulder, Colorado, USA, 1–159, doi:10.5065/D6FF3Q99, 1996.

Kiehl, J. T., Hack, J. J., Bonan, G. B., Boville, B. B., Williamson, D. L., and Rasch, P. J.: The National Center for Atmospherical Research Community Climate Model: CM3, J. Climate, 11, 1131–1149, 1998.

Kim, D. and Ramanathan, V.: Solar radiation budget and radiative forcing due to aerosols and clouds, J. Geophys. Res., 113, D02203, doi:10.1029/2007JD008434, 2008.

Kinne, S., Schulz, M., Textor, C., Guibert, S., Balkanski, Y., Bauer, S. E., Berntsen, T., Berglen, T. F., Boucher, O., Chin, M., Collins, W., Dentener, F., Diehl, T., Easter, R., Feichter, J., Fillmore, D., Ghan, S., Ginoux, P., Gong, S., Grini, A., Hendricks, J., Herzog, M., Horowitz, L., Isaksen, I., Iversen, T., Kirkevåg, A., Kloster, S., Koch, D., Kristjansson, J. E., Krol, M., Lauer, A., Lamarque, J. F., Lesins, G., Liu, X., Lohmann, U., Montanaro, V., Myhre, G., Penner, J., Pitari, G., Reddy, S., Seland, O., Stier, P., Takemura, T., and Tie, X.: An AeroCom initial assessment – optical properties in aerosol component modules of global models, Atmos. Chem. Phys., 6, 1815–1834, doi:10.5194/acp-6-1815-2006, 2006.

Kinne, S., O'Donnel, D., Stier, P., Kloster, S., Zhang, K., Schmidt, H., Rast, S., Giorgetta, M., Eck, T. F., and Stevens, B.: MACv1: a new global aerosol climatology for climate studies, J. Adv. Model. Earth Syst., 5, 704–740, 2013.

Kniffka, A., Stengel, M., and Hollmann, R.: Validation Report, SEVIRI cloud mask data set, Satellite Application Facility on Climate Monitoring, Satellite Application Facility on Climate Monitoring, 21 pp., available at: www.cmsaf.eu, doi:10.5676/EUM_SAF_CM/CMA_SEVIRI/V001, 2014.

Kok, J. F.: A scaling theory for the size distribution of emitted dust aerosols suggests climate models underestimate the size of the global dust cycle, P. Natl. Acad. Sci. USA, 108, 1016–1021, doi:10.1073/pnas.1014798108, 2011.

Kothe, S. and Ahrens, B.: On the radiation budget in regional climate simulations for West Africa, J. Geophys. Res., 115, D23120, doi:10.1029/2010JD014331, 2010.

Kothe, S., Dobler, A., Beck, A., and Ahrens, B.: The radiation budget in a regional climate model, Clim. Dynam., 36, 1023–1036, doi:10.1007/s00382-009-0733-2, 2011.

Kothe, S., Panitz, H.-J., and Ahrens, B.: Analysis of the radiation budget in regional climate simulations with COSMO-CLM for Africa, Meteorol. Z., 23, 123–141, doi:10.1127/0941-2948/2014/0527, 2014.

Kotlarski, S., Keuler, K., Christensen, O. B., Colette, A., Déqué, M., Gobiet, A., Goergen, K., Jacob, D., Lüthi, D., van Meijgaard, E., Nikulin, G., Schär, C., Teichmann, C., Vautard, R., Warrach-Sagi, K., and Wulfmeyer, V.: Regional climate modeling on European scales: a joint standard evaluation of the EURO-CORDEX RCM ensemble, Geosci. Model Dev., 7, 1297–1333, doi:10.5194/gmd-7-1297-2014, 2014.

Kunz, A., Spelten, N., Konopka, P., Müller, R., Forbes, R. M. and Wernli, H.: Comparison of Fast In situ Stratospheric Hygrometer (FISH) measurements of water vapor in the upper troposphere and lower stratosphere (UTLS) with ECMWF (re)analysis data, Atmos. Chem. Phys., 14, 10803–10822, doi:10.5194/acp-14-10803-2014, 2014.

Lewis, M. R., Carr, M.-E., Feldman, G. C., Esaias, W., and McClain, C.: Influence of solar radiation on the heat budget of the equatorial Pacific Ocean, Nature, 347, 543–545, doi:10.1038/347543a0, 1990.

Lamarque, J.-F., Bond, T. C., Eyring, V., Granier, C., Heil, A., Klimont, Z., Lee, D., Liousse, C., Mieville, A., Owen, B., Schultz, M. G., Shindell, D., Smith, S. J., Stehfest, E., Van Aardenne, J., Cooper, O. R., Kainuma, M., Mahowald, N., McConnell, J. R., Naik, V., Riahi, K., and van Vuuren, D. P.: Historical (1850–2000) gridded anthropogenic and biomass burning emissions of reactive gases and aerosols: methodology and application, Atmos. Chem. Phys., 10, 7017–7039, doi:10.5194/acp-10-7017-2010, 2010.

Laprise, R.: Regional climate modelling, J. Comput. Phys., 227, 3641–3666, 2008.

Markovic, M., Jones, C. G., Vaillancourt, P. A., Paquin, D., Winger, K., and Paquin-Ricard, D.: An evaluation of the surface radiation budget over North America for a suite of regional climate models against surface station observations, Clim. Dynam., 31, 779–794, doi:10.1007/s00382-008-0378-6, 2008.

Meirink, J. F., Roebeling, R. A., and Stammes, P.: Inter-calibration of polar imager solar channels using SEVIRI, Atmos. Meas. Tech., 6, 2495–2508, doi:10.5194/amt-6-2495-2013, 2013.

Mercado, L. M., Bellouin, N., Sitch, S., Boucher, O., Huntingford, C., Wild, M., and Cox, P. M.: Impact of changes in diffuse radiation on the global land carbon sink, Nature, 458, 1014–1017, doi:10.1038/nature07949, 2009.

Ming, Y., Ramaswamy, V., Ginoux, P. A., and Horowitz, L. H.: Direct radiative forcing of anthropogenic organic aerosol, J. Geophys. Res., 110, D20208, doi:10.1029/2004JD005573, 2005.

Mueller, R. and Träger-Chatterjee, C.: Brief accuracy assessment of aerosol climatologies for the retrieval of solar surface radiation, Atmosphere, 5, 959–972, doi:10.3390/atmos5040959, 2014.

Mueller, R., Matsoukas, C., Gratzki, A., Hollmann, R., and Behr, H.: The CM-SAF operational scheme for the satellite based retrieval of solar surface irradiance-a LUT based eigenvector hybrid approach, Remote Sens. Environ., 113, 1012–1022, doi:10.1016/j.rse.2009.01.012, 2009.

Mueller, R., Trentmann, J., Träger-Chatterjee, C., Posselt, R., and Stöckli, R.: The role of the effective cloud albedo for climate monitoring and analysis, Remote Sensing, 3, 2305–2320, doi:10.3390/rs3112305, 2011.

Nabat, P., Solmon, F., Mallet, M., Kok, J. F., and Somot, S.: Dust emission size distribution impact on aerosol budget and radiative forcing over the Mediterranean region: a regional climate model approach, Atmos. Chem. Phys., 12, 10545–10567, doi:10.5194/acp-12-10545-2012, 2012.

Nakajima, T. and King, M. D.: Determination of the optical thickness and effective particle radius of clouds from reflected solar radiation measurements, Part 1: Theory, J. Atmos. Sci., 47, 1878–1893, 1990.

NWCSAF: Algorithm Theoretical Basis Document for "Cloud Products" (CMa-PGE01 v3.0, CT-PGE02 v2.0 & CTTH-PGE03 v2.1), EUMETSAT Satellite Application Facility on Nowcasting and Shortrange Forecasting, SAF/NWC/CDOP/MFL/SCI/ATBD/01, Issue 3, Rev. 0, 17 May 2010, 2010.

Pal, J. S., Giorgi, F., Bi, X., Elguindi, N., Solmon, F., Gao, X., Francisco, R., Zakey, A., Winter, J., Ashfaq, M., Syed, F. S., Sloan, L. C., Bell, J. L., Diffenbaugh, N. S., Karmacharya, J., Konaré, A., Martinez, D., da Rocha, R. P., and Steiner, A. L.:

Regional climate modeling for the developing world: the ICTP RegCM3 and RegCNET, B. Am. Meteorol. Soc., 88, 1395–1409, 2007.

Posselt, R., Mueller, R., Stöckli, R., and Trentmann, J.: Spatial and temporal homogeneity of solar surface irradiance across satellite generations, Remote Sensing, 3, 1029–1046, 2011a.

Posselt, R., Müller, R., Stöckli, R., and Trentmann, J.: CM SAF surface radiation MVIRI Data Set 1.0 – monthly means/daily means/hourly means. Satellite application facility on climate monitoring, available at: www.cmsaf.eu, doi:10.5676/EUM_SAF_CM/RAD_MVIRI/V001, 2011b.

Posselt, R., Mueller, R., Stöckli, R., and Trentmann, J.: Remote sensing of solar surface radiation for climate monitoring-The CM-SAF retrieval in international comparison, Remote Sens. Environ., 118, 186–198, doi:10.1016/j.rse.2011.11.016, 2012.

Posselt, R., Müller, R., Trentmann, J., Stöckli, R., Liniger, M. A.: A surface radiation climatology across two Meteosat satellite generations, Remote Sens. Environ., 142, 103–110, doi:10.1016/j.rse.2013.11.007, 2014.

Ramanathan, V., Crutzen, P. J., Kiehl, J. L., and Rosenfeld, D.: Aerosols, climate, and the hydrological cycle, Science, 294, 2119–2124, doi:10.1126/science.1064034, 2001.

Ricchiazzi, P., Yang, S., Gautier, C., and Sowle, D.: SBDART: a research and Teaching software tool for plane-parallel radiative transfer in the Earth's atmosphere, B. Am. Meteorol. Soc., 79, 2101–2114, 1998.

Roebeling, R., Feijt, A., and Stammes, P.: Cloud property retrievals for climate monitoring: implications of differences between Spinning Enhanced Visible and Infrared Imager (SEVIRI) on METEOSAT-8 and Advanced Very High Resolution Radiometer (AVHRR) on NOAA-17, J. Geophys. Res., 111, D20210, doi:10.1029/2005JD006990, 2006.

Rummukainen, M.: State-of-the-art with regional climate models, Wiley Interdiscip. Rev. Clim. Chang., 1, 82–96, doi:10.1002/wcc.8, 2010.

Rutan, D., Rose, F., Roman, M., Manalo-Smith, N., Schaaf, C., and Charlock, T.: Development and assessment of broadband surface albedo from Clouds and the Earth's Radiant Energy System Clouds and Radiation Swath data product, J. Geophys. Res., 114, D08125, doi:10.1029/2008JD010669, 2009.

Sanchez-Lorenzo, A., Wild, M., and Trentmann, J.: Validation and stability assessment of the monthly mean CM SAF surface solar radiation dataset over Europe against a homogenized surface dataset (1983–2005), Remote Sens. Environ., 134, 355–366, doi:10.1016/j.rse.2013.03.012, 2013.

Schmetz, J., Pili, P., Tjemkes, S., Just, D., Kermann, J., Rota, S., and Ratierk, A.: An introduction to Meteosat Second Generation (MSG), B. Am. Meteorol. Soc., 977–992, 2002.

Slingo, A.: A GCM parameterization for the shortwave radiative properties of water clouds, J. Atmos. Sci., 46, 1419–1427, doi:10.1175/1520-0469(1989)046<1419:AGPFTS>2.0.CO;2, 1989.

Solmon, F., Giorgi, F., and Liousse, C.: Aerosol modelling for regional climate studies: application to anthropogenic particles and evaluation over a European/African domain, Tellus B, 58, 51–72, doi:10.3402/tellusb.v58i1.16792, 2006.

Stengel, M., Kniffka, A., Meirink, J. F., Lockhoff, M., Tan, J., and Hollmann, R.: CLAAS: the CM SAF cloud property data set using SEVIRI, Atmos. Chem. Phys., 14, 4297–4311, doi:10.5194/acp-14-4297-2014, 2014.

Stephens, G. L., Li, J., Wild, M., Clayson, C. A., Loeb, N., Kato, S., L'Ecuyer, T., Stackhouse, P. W., Lebsock, M., and Andrews, T.: An update on Earth's energy balance in light of the latest global observations, Nat. Geosci., 5, 691–696, doi:10.1038/ngeo1580, 2012.

Tessier, R.: The Meteosat Programme, ESA Bulletin 58, 45–57, 1989.

Teuling, A. J., Hirschi, M., Ohmura, A., Wild, M., Reichstein, M., Ciais, P., Buchmann, N., Ammann, C., Montagnani, L., Richardson, A. D., Wohlfahrt, G., Seneviratne, S. I., Mauder, M., and Foken, T.: A regional perspective on trends in continental evaporation, Geophys. Res. Lett., 36, L02404, doi:10.1029/2008GL036584, 2009.

Trenberth, K. E., Fasullo, J. T., and Kiehl, J.: Earth's global energy budget, B. Am. Meteorol. Soc., 90, 311–323, doi:10.1175/2008bams2634.1, 2009.

Trentmann, J., Müller, R., and Hollmann, R.: Algorithm Theoretical Basis Document, MSG Surface Radiation, Satellite Application Facility on Climate Monitoring, available at: www.cmsaf.eu, doi:10.5676/EUMETSAT_SAF_CM/CLAAS/V001, 2013.

Vautard, R., Gobiet, A., Jacob, D., Belda, M., Colette, A., Deque, M., Fernandez, J., Garcia-Diez, M., Goergen, K., Guttler, I., Halenka, T., Karacostas, T., Katragkou, E., Keuler, K., Kotlarski, S., Mayer, S., van Meijgaard, E., Nikulin, G., Patarcic, M., Scinocca, J., Sobolowski, S., Suklitsch, M., Teichmann, C., Warrach-Sagi, K., Wulfmeyer, V., and Yiou, P.: The simulation of European heat waves from an ensemble of regional climate models within the EURO-CORDEX project, Clim. Dynam., 41, 2555–2575, doi:10.1007/s00382-013-1714-z, 2013.

Wang, K., Dickinson, R. E., Wild, M., and Liang, S.: Evidence for decadal variation in global terrestrial evapotranspiration between 1982 and 2002: 2. Results, J. Geophys. Res., 115, D20113, doi:10.1029/2010JD013847, 2010.

Webster, P. J., Clayson, C. A., and Curry, J. A.: Clouds, radiation, and the diurnal cycle of sea surface temperature in the Tropical Western Pacific, J. Climate, 9, 1712–1730, doi:10.1175/1520-0442(1996)009<1712:CRATDC>2.0.CO;2, 1996.

Wild, M. and Liepert, B.: The Earth radiation balance as driver of the global hydrological cycle, Environ. Res. Lett., 5, 025203, doi:10.1088/1748-9326/5/2/025203, 2010.

Wild, M., Folini, D., Schär, C., Loeb, N., Dutton, E. G., and Koning-Langlo, G.: The global energy balance from a surface perspective, Clim. Dynam., 40, 3107–3134, doi:10.1007/s00382-012-1569-8, 2013.

Zakey, A. S., Solmon, F., and Giorgi, F.: Implementation and testing of a desert dust module in a regional climate model, Atmos. Chem. Phys., 6, 4687–4704, doi:10.5194/acp-6-4687-2006, 2006.

Zakey, A. S., Giorgi, F., and Bi, X.: Modeling of sea salt in a regional climate model: fluxes and radiative forcing, J. Geophys. Res., 113, D14221, doi:10.1029/2007JD009209, 2008.

Zanis, P., Douvis, C., Kapsomenakis, I., Kioutsioukis, I., Melas, D., and Pal, J. S.: A sensitivity study of the Regional Climate Model (RegCM3) to the convective scheme with emphasis in central eastern and southeastern Europe, Theor. Appl. Climatol., 97, 327–337, doi:10.1007/s00704-008-0075-8, 2009.

Zanis, P., Ntogras, C., Zakey, A., Pytharoulis, I., and Karacostas, T.: Regional climate feedback of anthropogenic aerosols over Europe using RegCM3, Clim. Res., 52, 267–278, doi:10.3354/cr01070, 2012.

Zeng, X., Zhao, M., and Dickinson, R. E.: Intercomparison of bulk aerodynamic algorithms for the computation of sea surface fluxes using toga coare and tao data, J. Climate, 11, 2628–2644, 1998.

Zubler, E. M., Folini, D., Lohmann, U., Lüthi, D., Schär, C., and Wild, M.: Simulation of dimming and brightening in Europe from 1958 to 2001 using a regional climate model, J. Geophys. Res., 116, D18205, doi:10.1029/2010JD015396, 2011.